

Fatigue Properties of Multi-directionally Forged Pure Titanium Plates and Thin Foils

ILHAMDI
1153812011

A Thesis Submitted to the
Graduate School of Engineering, Gifu University
in Partial Fulfillment of the
Requirements for the degree of
DOCTOR OF ENGINEERING

GIFU UNIVERSITY

Gifu, Japan

September, 2018

Fatigue Properties of Multi-directionally Forged Pure Titanium Plates and Thin Foils

ILHAMDI

A Thesis Submitted to the
Graduate School of Engineering
in Partial Fulfillment of the
Requirements for the degree of
DOCTOR OF ENGINEERING

Approved by the

Thesis Advisor

Professor Dr. Yoshihiko Uematsu

GIFU UNIVERSITY

Gifu, Japan

September, 2018

by

Ilhamdi

All Rights Reserved

Contents

Fatigue Properties of Multi directionally Forged Pure Titanium Paltes and Thin

Foils	i
Contents	iii
List of tables.....	vi
List of figures.....	vii
Acknowledgment	xiv
Chapter 1 Introduction	1
1.1 Background	1
1.1.1 Health issue and Titanium	1
1.1.2 Multi-Directionally Forging (MDF)	7
1.2 Synopsys of thesis	11
Chapter 2 Fatigue Behavior of Multi-Directionally Forged Commercial Purity Grade	
2 Ti Plate in Laboratory Air and Ringer`s Solution.....	13
Abstract.....	13
2.1 Introduction	14
2.2 Experimental details	16

2.2.1 Materials.....	16
2.2.2 Specimens and procedure.....	17
2.2.3 Microstructure and fatigue fracture observation	20
2.3 Results	21
2.3.1 Microstructures	21
2.3.2 Fatigue properties.....	26
2.3.3 Fractography.....	30
2.4 Discussions	34
2.4.1 Effect of saline environment.....	34
2.4.2 Fatigue mechanism.....	34
2.5 Conclusions.....	39
Chapter 3 Fatigue behavior of multi-directionally forged Ti thin foil with different thickness	41
Abstract.....	41
3.1 Introduction	42
3.2 Experimental details	45

3.2.1 Materials	45
3.2.2 Specimen and procedures.....	46
3.2.3 Fatigue crack propagation (FCP) test.....	49
3.3 Results	52
3.3.1 Tensile properties.....	52
3.3.2 Fatigue properties.....	53
3.3.3 Fractography.....	56
3.4 Discussions	65
3.5 Conclusions.....	69
Chapter 4 Conclusion	71
References	77
List of publication	81
Journal.....	81
International conference	81
National conference.....	81

List of tables

Table 1 Mechanical properties of MDFed CP Ti and TP35C.....	17
Table 2 Micro hardness vickers value of the MDFed CP Ti (measured on the nd plane).....	29
Table 3 Tensile properties of MDFed CP Ti thin foil.	53
Table 4 Relation tensile and fatigue strength of MDFed CP Ti thin foil.....	55
Table 5 Condition of last end of MDFed CP Ti grade 2 thin foil after fatigue test.....	68

List of figures

Fig. 1. Typical of bone fractures [2]	3
Fig. 2. Bio implant placement (a) external, (b) internal fixation [2]	3
Fig. 3. Schematic illustration of the mdf process with loading stress σ . The index number indicates the aspect ratio of the sample dimension [15].	9
Fig. 4. As received MDFed CP Ti and Fatigue specimen; (middle) MDFed CP TI, (down) TP35C	19
Fig. 5 Corrosion fatigue test apparatus.	20
Fig. 6 Macrottexture of the MDFed CP Ti plate.	22
Fig. 7 TEM nanograph of the MDFed CP Ti;(left) dominant equiaxed structure, (right) a few layered structure also exist	23
Fig. 8 SEM micrograph of the TP35C, white arrow appointed at bigger grain size	23
Fig. 9 EBSD analysis of TP35C on RD-TD plane; (A) IPF map, (B) pole figure (0001) plane.....	25
Fig. 10 Texture of MDFed CP TI on basal plane (0001) by EBSD.	25

Fig. 11 Schematic illustration of texture in the MDFed and TP35C plates.	26
Fig. 12 S-N diagram of the MDFed CP Ti and TP35C.	28
Fig. 13 Normalized S-N diagram of the MDFed CP Ti by Vickers hardness	30
Fig. 14 Fatigue fracture surfaces of TP35C: (a) overview, (b) magnified view at the crack initiation site ($\sigma_a = 190\text{MPa}$, $N_f = 1.4 \times 10^6$)	32
Fig. 15 Fatigue fracture surfaces of mdfed ti in laboratory air (surface crack initiation): (a) overview, (b) and (c) magnified views at the crack initiation site (σ_a $= 270\text{MPa}$, $N_f = 6.5 \times 10^5$, lot B)	32
Fig. 16 Fatigue fracture surfaces of MDFed ti in laboratory air (sub-surface crack initiation): (a) overview, (b) magnified views at the crack initiation site ($\sigma_a = 230\text{MPa}$, $N_f = 3.2 \times 10^7$, lot B).....	33
Fig. 17 Fatigue fracture surfaces of MDFed Ti in Ringer'S solution air (sub-surface crack initiation): (a) overview, (b) magnified views at the crack initiation site ($\sigma_a =$ 230MPa , $N_f = 8.9 \times 10^6$, lot A).....	33

Fig. 18 EDS analysis result: (a) SEM image of sub-surface crack initiation site, (b) Ti mapping, (c) EDS spectrum ($\sigma_a = 230\text{MPa}$, $N_F = 3.2 \times 10^7$, lot B).....	37
Fig. 19 EBSD analysis result: (a) SEM image of sub-surface crack initiation site, (b) pole figure of the rectangular area in fig. (a), (c) distribution of grain sizes ($\Sigma A = 230\text{MPa}$, $N_F = 3.2 \times 10^7$, lot B).....	38
Fig. 20 Fatigue fracture surface of MDFed Ti in laboratory air (sub-surface crack initiation): (a) overview, (b) magnified views at crack initiation site ($\sigma_a = 250\text{MPa}$, $N_F = 1.9 \times 10^6$, lot B).....	38
Fig. 21 Mechanism of MDF..	44
Fig. 22 As-received material of CP Ti thin foil grade 2 fabricated by MDF, supplied from Kawamoto Heavy Industry.....	46
Fig. 23 Specimen geometry of;(up) tensile test, (bottom) fatigue test	47
Fig. 24 Specimen preparation for tensile and fatigue test.	48
Fig. 25 Set up specimen for tensile and fatigue test.	49
Fig. 26 Specimen appearance for FCP test.	50

Fig. 27 A typical tensile test curve. specimen thickness is 50 μm	52
Fig. 28 S-N diagram of CP Ti thin foil fabricated by MDF	55
Fig. 29 Normalized S-N diagram of CP Ti thin foil fabricated by MDF	56
Fig. 30 SEM micrographs showing tensile failure surface of 13 μm foil specimen,(a) whole view, (b) magnified view at B, (c) magnified view at C, (d) magnified view at D.....	57
Fig. 31 SEM micrographs showing tensile fracture surface of 20 μm foil specimen, (a) whole view, (b) magnified view at B, (c) magnified view at C, (d) magnified view at D.....	58
Fig. 32 SEM micrographs showing tensile fracture surface of 30 μm foil specimen, (a) whole view, (b) magnified view at B, (c) magnified view at C, (d) magnified view at D.	58
Fig. 33 SEM micrographs showing tensile fracture surface of 50 μm foil specimen, (a) whole view, (b) magnified view at B, (c) magnified view at C, (d) magnified view at D.	59

Fig. 34 SEM micrographs showing fatigue fracture surface of 13 μm foil specimen, $\sigma_a = 250 \text{ MPa}$, $N_f = 1.4 \times 10^6$ cycles; (a) longitudinal fracture line, (b) magnified view at B, (c) magnified view at C, (d) magnified view at D.....	61
Fig. 35 SEM micrographs showing fatigue fracture surface of 30 μm foil specimen, $\sigma_a = 290 \text{ MPa}$, $N_f = 181,602$ cycles; (a) longitudinal fracture line, (b) magnified view at B, (c) magnified view at C, (d) magnified view at D.....	62
Fig. 36 SEM micrographs showing fatigue fracture surface of 50 μm foil specimen, $\sigma_a = 270 \text{ MPa}$, $N_f = 1.3 \times 10^5$ cycles; (a) longitudinal fracture line, (b) magnified view at B, (c) magnified view at C, (d) magnified view at D.....	63
Fig. 37 Typical crack propagation line on FCP test specimen	64
Fig. 38 Typical crack propapagation curve. Specimen thickness of 13 μm	64
Fig. 39 FCP test result of specimen thickness of 13 μm	65
Fig. 40 Appearance of cross section of FCP test. Specimen thicknee of 13 μm	69

Acknowledgment

In the name of Allah, the Most Gracious and the Most
Merciful

The first, *Alhamdulillah*, praise and thank you belong to Allah the Almighty. Praise Him all day for what is and what was making it possible for me to complete my Ph.D. course at Uematsu-Kakiuchi laboratory of Gifu University, Japan. All the hurdles and difficulties during this work were only able to overcome by only from His permission.

My special thanks to my supervisor Professor Dr. Yoshihiko Uematsu, you have been the best mentor for me. I would like to thank you for gently guidance, encouraging my research and for allowing me to grow as a researcher.

I am would also like to thank so much to Asc. Professor Dr. Toshifumi Kakiuchi, and Professor Minoru Yamashita as committee member on my research, thanks you for the comments and advice on my research, especially during the defense which was may disturb your daily schedule.

Big thank you I should address to Professor Dr. Masaki Nakajima, for warm welcome and advices on y research. I will not forget the kindness of Dr. Masayuki Akita, thank you so much Akita-san. All Uematsu laboratory students especially for

my former team mate; Tomohiko Fukihara and Kenichi Yokohama, Tamada-san, and former member of B-room for their humor, support and encouragement, .

I also would like to express my appreciation and thanks to Professor Gunawarman, my parents, my grandparents, my adopted parents, all my brothers and sisters, my parents-in-law and my lovely wife and daughters and unborn baby for their presences, support and prayers.

And the last but not the least, thank you very much to Indonesian government that give me financially support to pursue this doctoral program through scholarship of Directorate General Resource for Science, Technology and Higher Education (BPPLN-Dikti).

Chapter 1 Introduction

1.1 Background

1.1.1 Health issue and Titanium

Health is amenity for living thing on the earth as well as life itself. Taking care of the body healthy is play important role in the humankind history. Healthier generations have been made a better future than less health generation. It is common sense that developed countries have higher level in human health than developing countries. For comparison, based on the Legatum prosperity index [™] 2017, health index of Japan is the best four, while Indonesia on 101 among 184 countries [1]. This index is measured based on three area i.e. basic physical and mental health, health infrastructure and preventive care.

Human body could be divided into skin/derma, soft tissue (meat, blood vessel, neuro, etc) and hard part (bone, skull and teeth). The human body may get injuries from some accidents or intentional thing. The injuries could be appeared as; cut or removed skin, cut or bleeding tissue, and cracked or broken hard part. Fortunately, human body also has ability to experience recovery process after injury even very limited degree or low rate. Usually skin and soft tissue are faster in recovery than hard part.

The hard part constructed from mainly calcium for hard outer. This outer covers some void with semi liquid and neuron system in the inside part. Both of bone, skull and teeth have this characteristic. Teeth are the most exposed hard part while skull is covered by skin and bone by skin and soft part. So, broken tooth is more difficult to get natural healing compare to fracture bone or skull. Fortunately, massive and intensive research and development technology had been useful to overcome difficulties on the healing and recovery of the broken part human body.

Some typical crack or fracture of the bone could be seen in Fig. 1. Higher degree of damage on the bone required longer time to take recovery. New bone will be reformed from deposition calcium on the tip of broken bone. Calcium resource may take from nutritious elements of foods or supplements. Because new bone is not as hard as the existing, some plates or rods are needed to act as support during its growth and recovery. This support system is known as bio implant fixation as shown in Fig. 2. This support system can be an external or internal placement to the broken bone, depending on the damage level. A simple fracture on the bone could be fixated using external fixation, but more severe damage may use the internal fixation. Normally, this support system could be removed after new bone becomes as hard as the existing bone, about a few weeks or several months after operation.

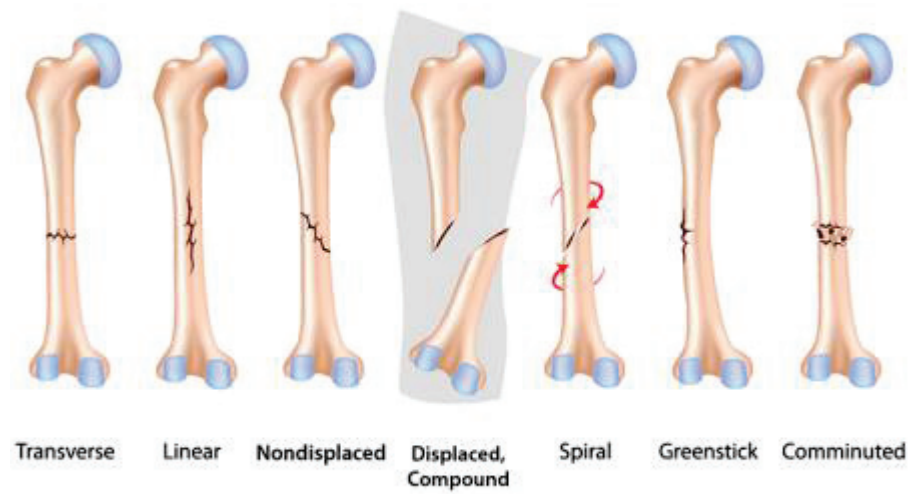


Fig. 1. Typical of bone fractures [2].

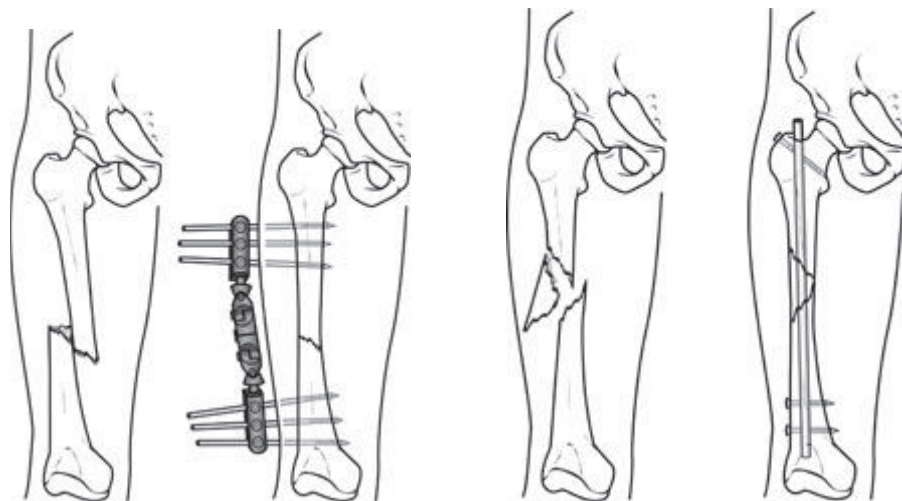


Fig. 2. Bio implant placement (a) external, (b) Internal fixation [2]

From the viewpoint of medical engineering, bio implant should have equal characteristic with the existing bone; namely mechanical strength, Young's modulus, elongation and fatigue properties. On the other hand, bio implant should not cause

some bad responses to the surrounding soft tissues it contacted with. At low level the response could be allergic reaction, but in higher level it can be toxicity reaction. Naturally, some metal can be dissolved (corroded) into their environment through electrochemical reaction facilitated by some wet or solution. So that, it is desired that bio implant should have a very good resistance against corrosion and free from allergic-element and toxin-element.

However in beginning of time, human thought very simple for replacing the lost teeth or fixing the broken part of their body. Saini et. al. mentioned that implant was traceable in the ancient era of Egypt and South America civilization; a skull with artificial tooth from dark stone was found from Columbian era [3]. The first recorded bone grafting operation was in 1668 by Dr. Van Meekereen. Since 1800, some natural metals such as aluminum, silver, brass, red copper, magnesium, gold and soft steel plated with gold and nickel, and titanium were used as dental implant.

In the modern era, titanium was used in surgeries from 1950's for inner body devices, internal fixation and medical instrument. Titanium and its alloys can be used as bio implant from head to toe of the patient. Titanium can stay in the human body up to 20 years as bio implant, or even longer as dental implant. The main reasons of using Titanium as bio implant are biocompatibility with human

tissue and bone, high corrosion resistance, and nontoxicity. Other good properties are relatively low specific gravity of 4.5 (~50% of copper, ~60% of iron), comparable mechanical strength to steel with half of Young's modulus, and easily formed like a stainless steel. Therefore titanium and its alloys become main metal for bio implant.

Based on Institute for Energy Technology (IFE) titanium could be divided into two big categories; commercially pure titanium and titanium alloys [4]. The commercially pure titanium is abbreviated as CP Ti, and has four main grade based on their purity. CP Ti Grade 1 is unalloyed titanium which offering optimum ductility and cold formability with useful strength, high-impact toughness, excellent weldability, high corrosion resistant in oxidizing and mild corrosion resistant in reducing environments, including chlorides. Grade 2 is the most widely used CP Ti in all product forms for industrial service, offers an excellent balance of moderate strength and reasonable ductility, and comparable corrosion properties with grade 1. Grade 3 has optimum ductility and cold formability with useful strength, high-impact toughness, and excellent weldability. CP Ti Grade 4 provides corrosion resistance, strength and fatigue characteristics that compare favorably to those of nickel and steel alloys. It is the strongest grade with moderately formable alloy with

good ductility.

All the CP Ti is typically α -phase microstructure with small amount of spheroid β -phase. Their mechanical properties can be resumed as follow; mechanical strength varies between 240-685 MPa, elongation in 50 mm is between 24-15% and Young's modulus is about 102-104 GPa. This modulus is lower than the other metallic biomaterial like stainless steel (206 GPa) and cobalt type alloys (240 GPa), but still much higher than that of bone which is in between 17 to 28 GPa [5].

Titanium alloys have big range variety, from grade 5 to grade 29. Some high numbers of grades of Ti have equal mechanical properties with CP Ti, but better properties in some aspects. Titanium grade 7, 16 and 26 are equal with CP Ti grade 2 on mechanical properties, but presence of a few Pd in the grade 7 and 16 or a few Ru in the grade 26 made their corrosion resistance better [4].

Based on the microstructure constituent, they could be divided into alpha-beta phase alloys, and beta-phase alloys [4]. The α -phase is a Hexagonal Closed Packed (HCP) crystal lattice structure, while the β -phase is in Body Centered Cubic (BCC) form. In the process, α -phase may be stabilized by Al, Ga, N and O, in which Mo, V, W, Ta and Si may be effective to stabilize β -phase.

Ti alloys have mechanical strengths up to 1100 MPa, much higher compare to CP Ti. The nearest alloy to commercially pure titanium is grade 5, Ti-6Al-4V (sometimes abbreviated as Ti64). This alloy is widely used as bio material for implants, both in dental or surgery purposes. Because of lack in stress corrosion cracking (SCC), Ti64 was modified into Ti-6Al-4V ELI (Extra Low Interstitial) by reducing its interstitial elements (O, N, C). The latter alloy is also widely used as a structural bio implant for replacing failed hard part like hip joint or for screw and crown in dental implant, because of its excellent mechanical properties, and corrosion resistance [6, 7].

1.1.2 Multi Directionally Forging (MDF)

There are many ways to improve mechanical properties of engineering material such as alloying, precipitation, cold working etc. Metal alloys are mainly strengthened through alloying, heat treatment or cold working. However, pure metal is difficult to be strengthened through above mentioned methods. On the others hand, adding some elements (alloying) into a dominant/base metal will change the properties of metal itself; corrosion properties of Ti64 are slightly different compare to CP Ti, but its mechanical strength is significantly increased.

At some last decades, many researchers are developing severe plastic deformation (SPD) methods on pure or alloy metal with low strength. The SPD techniques can be said as massive development of the cold working process with very high applied strain on subjected material. Cold working in maximum can provide about 0.2 of strain on the material during the process. But, SPD can achieve between 0.6 till 1 of strain in one step of its process.

Y. Estrin and A. Vinogradov mentioned that “the modern-day history of SPD technology started in the seminal work of P.W. Bridgman who developed the scientific grounds and techniques for materials processing through combination of high hydrostatic pressure and shear deformation” [8]. It was in the early of 1950`s. Later, Valiev et al defined SPD process as “any method of metal forming under extensive hydrostatic pressure that may be used to impose a very high strain on a bulk solid without the introduction of any significant change in the overall dimensions of the sample and having the ability to produce exceptional grain refinement” [9].

Some existing SPD techniques could be listed as follows; Equal Channel Angular Pressing (ECAP) [10], High Pressure Torsion (HPT) [11], Multi Directionally Forging (MDF) [12], and Accumulated Roll Bending (ARB) [13]. The most important

point in SPD techniques is their ability to produce fully dense or homogenous grain refinement in range of submicron (100-1000 nm) to nanometer (<100nm) (also known as ultra-fined grain, UFG), and bulk-scale work-pieces.

Among them, MDF is seemed to be the best suited to apply on industrial work to produce large-size billets with UFG structures and was successfully applied to a wide range of materials [14]. Representative mechanism for MDF process could be seen in Fig. 3. Multiple free-forging operations include repeated setting in three orthogonal directions consecutively along Z, Y and X-axis. All three forging is named as one pass or one cycle. In that figure, index of specimen dimension ratio is also shown, and size back to original after one pass. Total strain in one pass of MDF on AZ61 magnesium alloys is about 0.8 [12], a much higher number than conventional cold working.

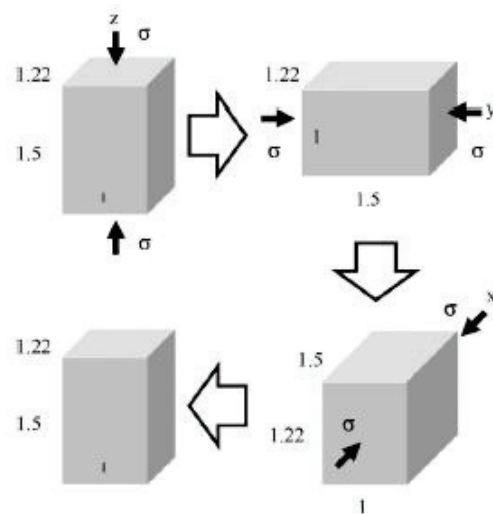


Fig. 3. Schematic illustration of the MDF process with loading stress σ [15].

Usually, MDF is conducted under the elevated temperature of $0.1-0.5T_m$, where T_m is the melting temperature. Therefore grain refinement in the MDF material is associated with continuous dynamic recrystallization as reported by Belyakov et al. and Takayama et al [16, 17]. Thanks to elevated temperature, MDF also could be applied on refinement of brittle materials, and enable to use low specific loads on tooling involved.

One of the brittle materials that was successfully strengthened through MDF is CP Ti, developed by our collaborator, Professor H. Miura. Mechanical strength of CP Ti grade 2 was successfully increased up to ~ 1000 MPa, in the range of Ti alloys such as Ti-6Al-4V. It is good news for the application in biomedical devices and bio implants. It is well known that Ti-6Al-4V has aluminum and vanadium as alloying elements; to increase mechanical strength and stabilize the alloys. However, presence of Al and V in Ti-6Al-4V sometimes raise allergic reaction on patient after bio implant set up. Naturally, both free from allergic element and significantly improved mechanical strength after MDF made CP Ti more proper materials for bio implant purposes.

Above studies showed the significance of MDF in the strengthening methods of metals as one of the developed SPD techniques. In term of bio implant such as pen

in broken bone fixation or artificial hip joint, bio implant will experience rhythmic loading for long time or typical fatigue loading. On the other hand, it is well known that before using as structural component, material should have adequate mechanical properties and a well understood fatigue behavior. However, study about fatigue behavior of the titanium after MDF is quite limited.

In this study, the sheets and foils of CP Ti from Kawamoto Heavy Industry, that were produced by MDF, was used for the specimens. Fatigue behavior of 1 mm MDFed sheet, and 50, 30, 20, 13 μm MDFed foils was investigated.

1.2. Synopsis of thesis

The present thesis contains two major parts: “Fatigue Behavior of Multi-Directionally Forged Commercial Purity Grade 2 Ti Plate in Laboratory Air and Ringer’s Solution” and “Effect of Thickness on Tensile and Fatigue Properties of Multi-Directionally Forged Commercial Purity Grade 2 Ti Thin Foil”. The thesis overall structure is as follows:

Chapter 1 presents an overview of the background information related to the present study in order to serve as a prelude to the topics covered in later chapters.

In Chapter 2 “Fatigue Behavior of Multi-Directionally Forged Commercial Purity Grade 2 Ti Plate in Laboratory Air and Ringer’s Solution”, fatigue properties of MDFed CP Ti grade 2 will be discussed. Subsequently, texture and mechanical

properties were examined. The fatigue strength was evaluated, and initial of fracture mechanism were discussed based on fracture surface and microstructure observation.

In Chapter 3 “Effect of Thickness on Tensile and Fatigue Properties of Multi-Directionally Forged Commercial Purity Grade 2 Ti Thin Foil”, fatigue and tensile tests were conducted using CP Ti foils with different thicknesses to investigate fatigue behavior and its relation with tensile properties. In addition, a fatigue crack propagation (FCP) tests were also conducted on the thinnest and thickest CP Ti foils. Fatigue behavior was discussed based on experimental observation.

The last Chapter 4 is summary of the overall research result and finding of the theses.

Chapter 2 Fatigue Behavior of Multi-Directionally Forged Commercial Purity Grade 2 Ti Plate in Laboratory Air and Ringer's Solution

Abstract

Fatigue tests of ultrafine-grained pure Ti plates fabricated by multi-directional forging (MDFing) were conducted in laboratory air and in physiological saline. The plate with 1 mm in thickness was developed aiming at dental implant application. The fatigue strengths of multi-directionally forged commercially pure titanium (MDFed CP Ti) plates in laboratory air were higher than those of conventional rolled pure Ti plates. It could be attributed to the much finer grains evolved by MDFing. In the very high cycle fatigue (VHCF) regime, sub-surface crack initiation was observed in the MDFed CP Ti, and the sub-surface crack initiation mechanism was related to the inhomogeneity of microstructure, instead of inclusion. The corrosion fatigue strengths in Ringer's solution were comparable to those in laboratory air, indicating high corrosion resistance of MDFed CP Ti.

Keywords: Commercially pure titanium, multi-directionally forging, fatigue strength, corrosion fatigue, fish-eye, inhomogeneity of microstructure.

2.1 Introduction

Pure titanium and titanium alloys are most attractive metallic materials for biomedical application. Ti-6Al-4V which is considered as grade 5, one grade higher than pure Ti [18], has been used as structural materials for bio implants due to its high strengths and superior corrosion resistances [19]. This is because high strength can be achieved by adding alloy elements such as Vanadium into pure Ti. Fleck and Eifler revealed that the fatigue strengths of commercial purity grade 2 Ti were about a quarter of those of Ti-6Al-4V [20]. However, from the viewpoint of long-term use in human body, the use of alloy additives could sometimes induce metal ion stimulus known as metal allergy. Thus, pure Ti without any alloy elements is better than Ti alloys for long-term use as implants. Therefore, it is required to increase the strength of pure Ti which is inferior in absolute strength to Ti alloys. Consequently, strengthening of pure Ti without any alloy elements became important issue for the application of medical implants.

Recently, severe plastic deformation (SPD) methods such as equal channel angular pressing (ECAP) [3] and high pressure torsion (HPT) [4] attract attention as strengthening methods of metals. Multi-directional forging (MDFing) is one of the SPD methods, in which materials are forged with changing forging axes for 90

degrees pass by pass [5-7]. The SPD methods were developing on wide range alloys and pure metals such as copper, aluminum, magnesium, titanium, even on steel [8]. The major advantage of MDF is fabrication of large component. One of the researches reported this potential by Kaibyshev who developed MDF on VT6 titanium alloy [9].

Recently, high strength pure Ti with high corrosion resistance was fabricated by combined process of MDFing and rolling (here after denoted as MDFed CP Ti for simplicity) for dental implants application. This material was developed in collaboration with dentistry researchers, and trial dental crowns were successfully fabricated [21,22]. For the long-term durability of the implants, it is important to understand high cycle fatigue (HCF) properties of severely deformed pure Ti, and also corrosive environment impacts on the implant. However, the fatigue behavior of MDFed pure Ti in air and in corrosive environment is not studied. Therefore, in this study, we used ultra-fined grained commercially pure Ti grade 2; which was produced by multi-directionally forging method to investigate fatigue properties. The fatigue test environments are in laboratory air and in Ringer's solution to simulate the dental implant condition.

2.2. Experimental Details

2.2.1. Materials

The material used is an industrial grade pure Ti plate of grade 2 (denoted as MDFed CP Ti as already mentioned above) which was processed by MDFing at Kawamoto Heavy Industries, Japan. The as-received MDFed CP Ti plates have the length of 750 mm, width of 70 mm and thickness of 1 mm as shown in Fig. 4. The coordinate of rolling direction (RD), transverse direction (TD) and normal direction (ND) is defined as shown in the figure. As a reference material, conventional cold-rolled commercial purity grade 2 Ti was used, which was classified as TP35C in accordance with JIS (Japanese Industrial Standard) H4600. The as-rolled plates have the length of 382 mm, width of 47 mm and thickness of 0.15 mm.

Here, MDF is a method of repeatedly applying a constant forging pass-to-path distortion $\Delta\epsilon$ to a short-shape test piece having a certain constant ratio on three sides, while changing the compression load direction by 90 °, and adding huge strain.

Mechanical properties of the MDFed CP Ti and TP35C are summarized in Table 1. MDFed CP Ti possesses higher tensile strength and proof stress than TP35C. This static strength of MDFed CP Ti is comparable with Ti-6Al-4V which is at the range of 860-976 MPa [10]. It should be emphasized that the elongation is larger in

MDFed CP Ti than in TP35C, indicating that not only tensile properties but also ductility were improved by MDFing. Increase in ductility means MDFed CP Ti has higher possibility to be formed than TP35C or, even compare to Ti-6Al-4V which only have elongation in the range of 5-15% [10].

Table 1. Mechanical properties of MDFed CP Ti and TP35C.

Materials	Yield strength σ_y (MPa)	Tensile strength, σ_B (MPa)	Elongation, (%)	Vickers Hardness, (HV)
MDFed CP Ti	920	766	18	316
TP35C	746	619	7	258

2.2.2. Specimens and procedures

Fatigue specimens were taken out from the as-received materials in the rolling direction by wire electrical discharge machining according to configuration in Fig. 4. The MDFed CP Ti specimens have the gage length of 20 mm and width of 8 mm. The keyholes on the grip section aimed to facilitate fastening mechanism during fatigue test. The testing machine used is a 50 kN capacity electro-hydraulic fatigue testing machine. Due to the thin thickness of the as-received material, tension-compression fatigue tests could not be conducted. Therefore, a tension-tension fatigue test with the sinusoidal load wave form was conducted

under the stress ratio $R = \sigma_{\min}/\sigma_{\max}$ was set to be 0.1 and the frequency of 10 Hz. These fatigue tests were conducted in two different environments; i.e. an atmospheric laboratory air with ambient temperature and in a Ringer's solution with controlled temperature for corrosion fatigue test. Ringer's solution contains 8.6 g/l NaCl, KCl 0.3 g/l, 0.33 CaCl₂.2H₂O. The solution temperature was kept at 37 °C by thermostat and kept flowing during the test by a metering pump as shown in Fig. 5. Before the fatigue test, edge of specimen was mechanically polished with progressively finer emery papers and alumina paste till a mirror-like surface achieved.

The as-received MDFed CP Ti was 3 plates (here on denoted as lot). The fatigue properties between lots are slightly different. Thus, hardness of a mirror-like lot specimen was measured by micro Vickers Hardness Method with the loading of 300 N for 30 seconds to normalized S-N graph. The total number of indentation was 20. The obtained average hardness value was used for normalized S-N graph.

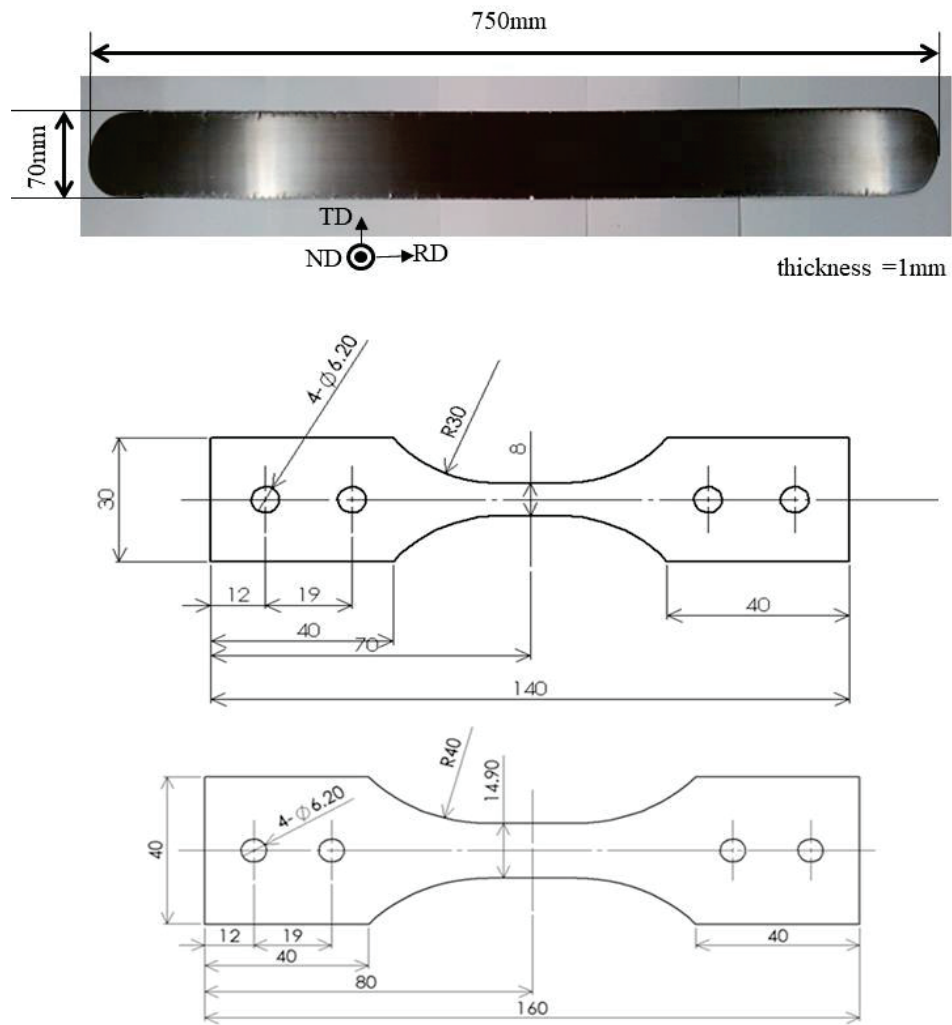


Fig. 4. As received MDFed CP Ti and fatigue specimen configuration; (middle)

MDFed CP Ti, (down) TP35C

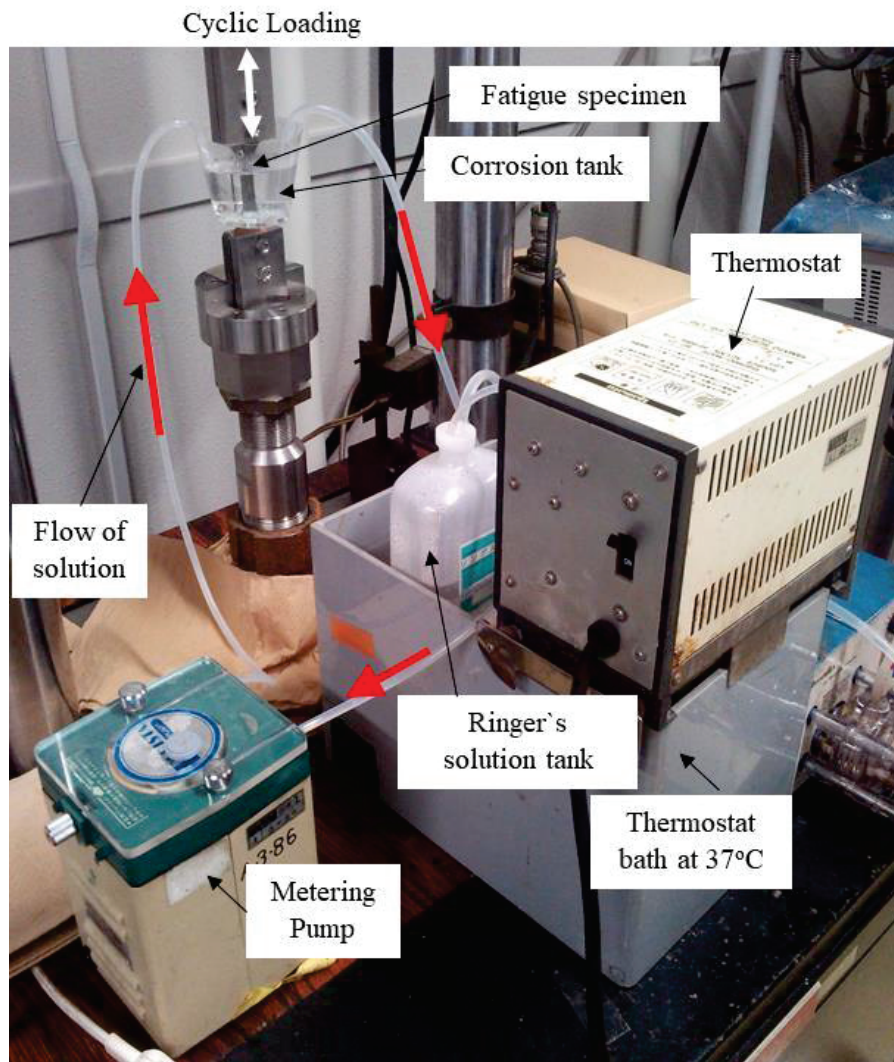


Fig. 5. Corrosion fatigue test apparatus

2.2.3. Microstructure and fatigue fracture observation

Microstructure of TP35C was clearly observed with scanning electron microscope (SEM) while no structure image was achieved on the MDFed CP Ti. Thus, observation on the MDFed CP Ti was conducted under transmission electron microscope (TEM). The microstructure detail will be described in the section 2.3.1.

Before observation, a mirror-like surface of the TP35C specimen was etched in $2\%HF + 3\%HNO_3 + 95\%$ distilled water.

Part with fatigue fracture surface in size about 10 mm in height was cut off from specimen body. After cleaned by alcohol in ultrasonic cleaner, it was observed using SEM of JEOL JSM6060 at accelerated voltage of 15 kV.

In order to observe the site near fatigue crack initiation, some measuring was conducted; EDX Hitachi S-4300 SE to calculate chemical element distribution and EBSD to determine grain size. Before analysis with EBSD, the fish-eye fracture surface was polished by alumina suspension, and then ion milled by HITACHI: IM-3000 Flat Milling System. X-ray diffraction (XRD) analysis was performed to observe the texture of the microstructure using RIGAKU SmartLab.

2.3. Results

2.3.1. Microstructures

Fig. 6 shows the macro texture of the MDFed CP Ti plate observed by SEM. Each plane has separated characteristic; LD plane showed a tighter bundle of layered tissue than in TD and LD plane. Some micro etch pits were found in LD plane with diameter of 4 mm. These holes are suspected to be corrosion site during fatigue

test within saline environments. It might be a crack initiation site. No grain is seen through optical microscope due to ultrafine grained microstructure by MDFing.

In order to verify existence of the ultrafine grain, TEM was used to observe microstructure of MDFed CP Ti as shown in Fig. 7. It is composed of homogeneous equiaxed ultrafine grains with the average size of 200 nm as in Fig 7 (left). However, a few parts of layered structures were also seen in Fig 7 (right). For comparison, the microstructure of the conventional rolled CP grade 2 Ti is also displayed in Fig. 8, which was observed by an optical microscope. On the other hands, some coarse grains are recognized in TP35C revealing inhomogeneity in the microstructure. Arrows in Fig 8 indicate the typical coarse grains. These coarse grains have the size about 20 μm .

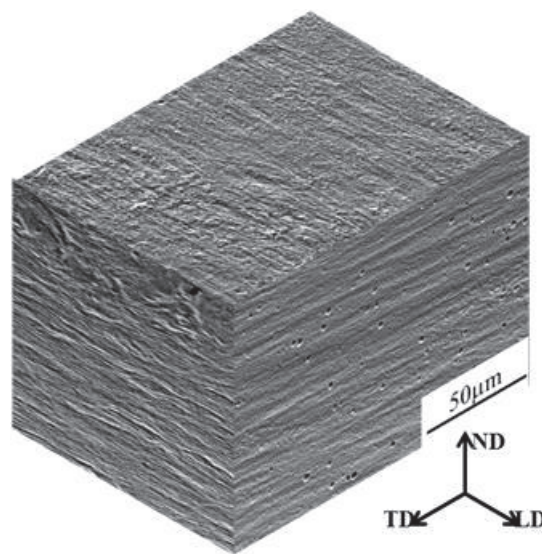


Fig. 6. Macrotexture of the MDFed CP Ti plate.

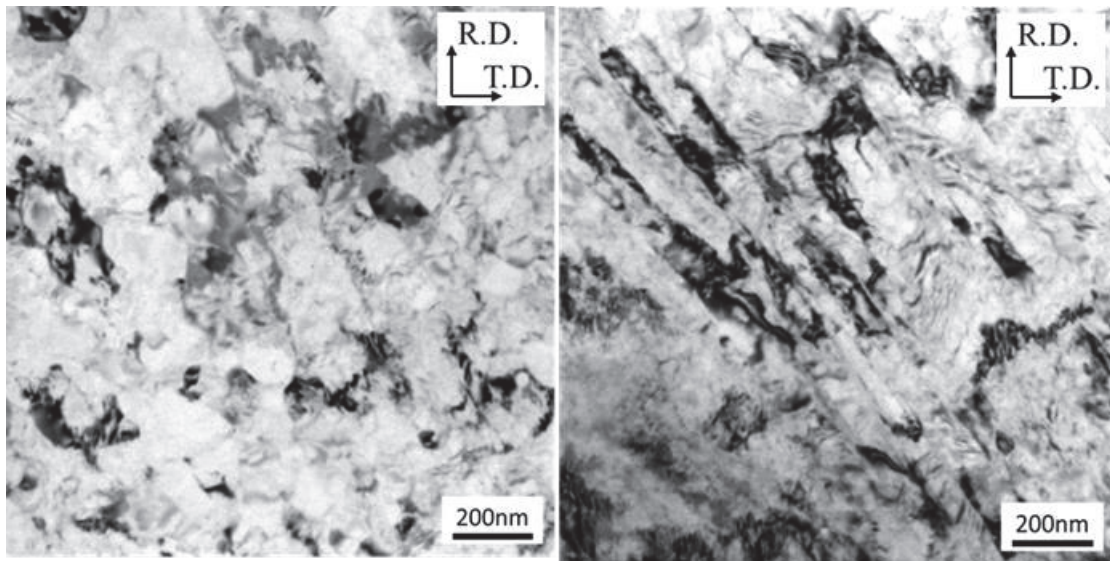


Fig. 7. TEM nanograph of the MDFed CP Ti;(left) dominant equiaxed structure, (right) a few layered structure also exist.

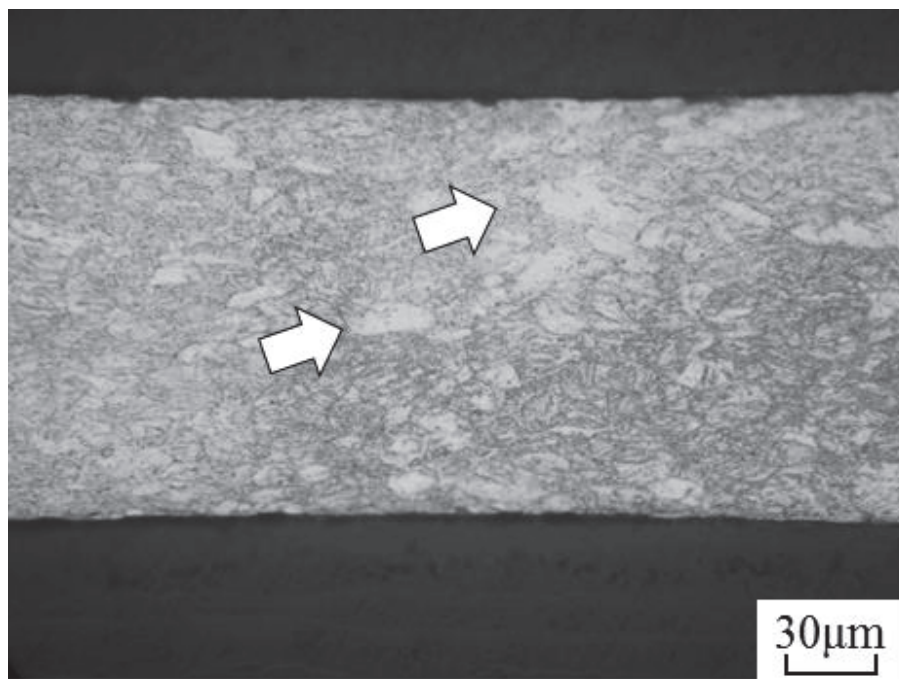


Fig. 8. SEM micrograph of the TP35C, white arrow appointed at bigger grain size

EBSD analysis was performed on the surface of the plate (RD-TD plane) as shown in Fig. 9(a). It can be seen that the microstructure consists of some fine and coarse grains, in which the size of coarse grains was about 30 μm . Fig. 9(b) is the pole figure of (0001) plane. It reveals that the typical texture is formed by the cold rolling procedure. The TEM observation of MDFed Ti is shown in Fig. 10(a). The SPD by MDFing had resulted in very fine and homogeneous microstructure with an average grain size of 200 nm. Although EBSD was performed on the surface of the MDFed Ti plate, clear Kikuchi bands could not be detected due to the large residual strain induced by MDFing. Therefore, XRD analysis was performed on the surface of the MDFed Ti plate. Fig. 10(b) reveals the pole figure of (0001) plane, where the texture was confirmed to be similar to that of TP35C (Fig. 9(b)), where two [0001] axes symmetrically inclined about 16 to 34 degrees from ND axis. It is interesting to know, therefore, that a same texture develops irrespective of grain size. The texture developed in both plates is schematically drawn in Fig. 11. Dyakonov et al. reported similar texture in the heavily cold-rolled pure Ti, in which the rolling reduction was 95% [23].

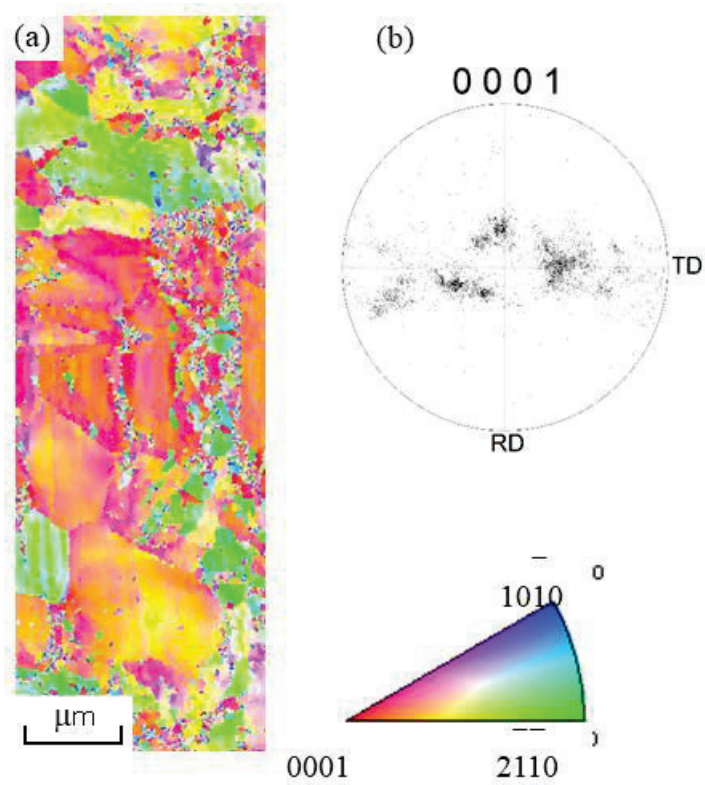


Fig. 9. EBSD analysis of TP35C on RD-TD Plane; (a) IPF map, (b) pole figure (0001) plane.

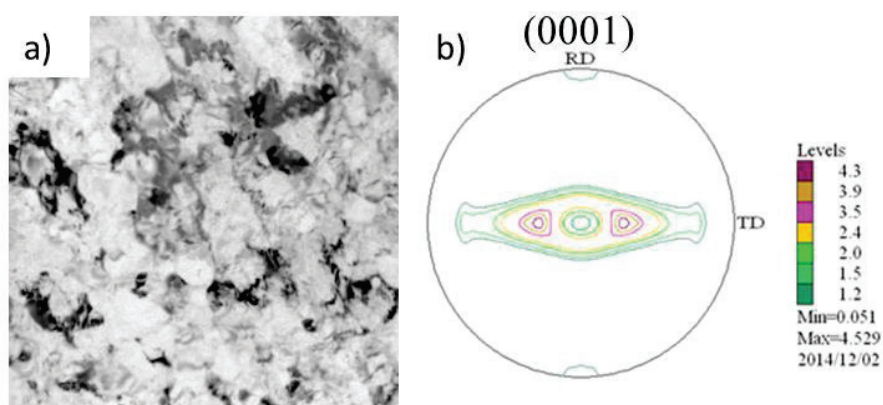


Fig. 10. Texture of MDFed CP Ti on basal plane (0001) by EBSD

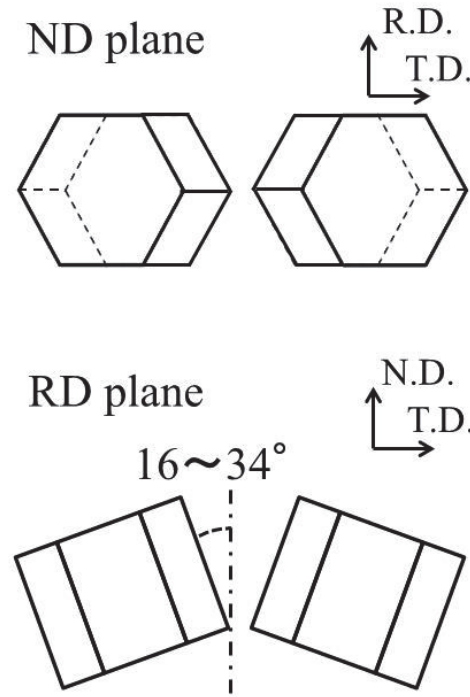


Fig. 11. Schematic illustration of texture in the MDFed and TP35C plates.

2.3.2. Fatigue Properties.

Fig. 12 indicates the relationship between applied stress amplitude, σ_a , and number of cycles to failure, N_f , namely $S-N$ curve. Thickness of TP35C is 0.15 mm and MDF material is 1 mm, but because both materials are thin, they are considered to be in the same plane stress state. Fatigue test result of MDFed CP Ti in laboratory air and in Ringer's solution as shown by symbol of hollow marks (open) and solid marks (closed), respectively. The asterisk marks "*" in the figure will be mentioned in the next section.

Focusing on the test results in laboratory air, the MDFed CP Ti specimens exhibit higher fatigue strengths than the conventional rolled TP35C. The higher fatigue strengths of MDFed Ti could be attributed to the ultrafine grains induced by

MDFing. In the present case, the thickness of the plates is 0.15 and 1 mm for TP35C and MDFed Ti plates, respectively. But the point is that TP35C is deeply-cold-rolled (highly-work-hardened) plate into the thickness of 0.15 mm. It means that the MDFed Ti plate has higher fatigue strengths than the deeply-cold-rolled TP35C plate. Furthermore, both plates with the thickness of 0.15 and 1 mm are under the same stress state, namely under plane stress condition. Thus, the thickness itself has little effect on the fatigue strengths. The authors conducted fatigue tests of MDFed Ti thin films with the thickness of 15, 20, 30 and 50 μm , and proved that the fatigue strengths of the plate and films were nearly comparable [24].

On the other hand, the results in Ringer's solution have both of higher and lower strength than the results in air, and have large scatter. This scatter is attributed to the fact that specimens were taken from the different lots which fatigue specimens were prepared. That is, although the results of the lots A, B, and C are distinguished and displayed in the figure, it can be seen that the variation is small as the S-N curve of each lot. Especially, only the lot A is tested in both air and in Ringer's solution, but the result is almost one curve. It can be considered that there is no reduction in fatigue strength in Ringer's solution, and it proves the long-term durability of the MDFed Ti plates in human body. It should be noted that fatigue strengths could be approximated by the S-N curves for each lot. In general, MDFed materials have stable strength due to the repeated severe plastic deformation [25], thus the different strengths between two lots might be attributed to the final rolling process.

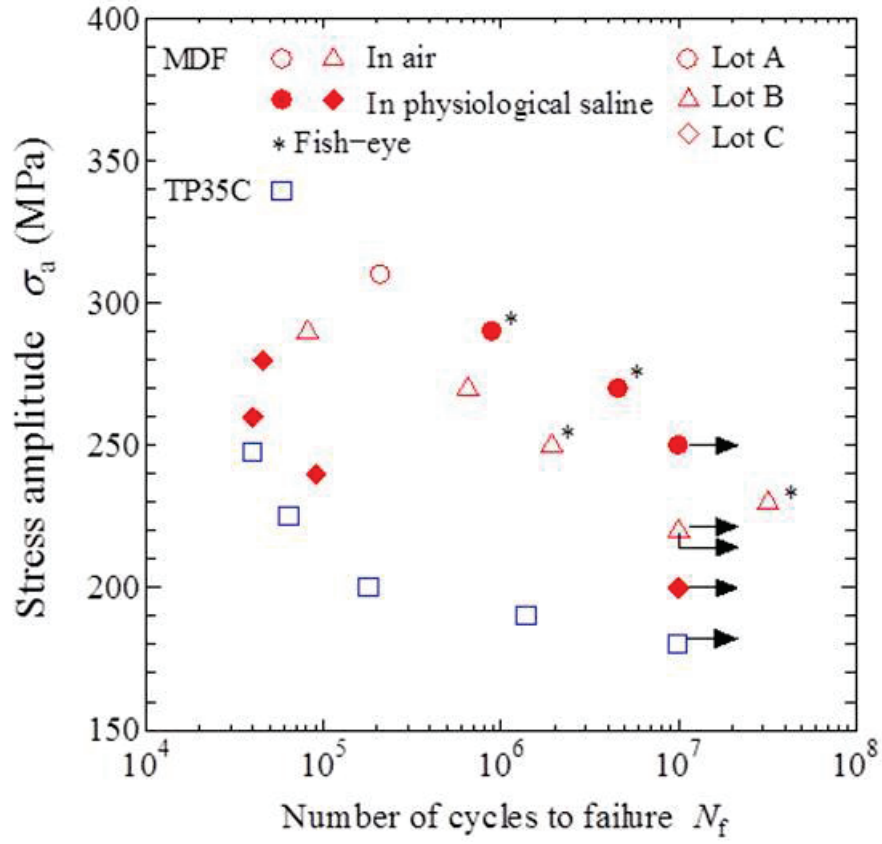


Fig. 12. S-N diagram of the MDFed CP TI and TP35C.

In order to verify the difference of the fatigue strengths between the lots A, B and C, their hardness were determined with micro Vickers method separately. The result was summarized in Table 2. All measurements were done on the longitudinal plane of the plates. The lot A exhibit higher hardness value than the Lots B and C. However their variation are coincide each other. It can be considered that the hardness has a good agreement with the fatigue strength.

Table 2. Micro hardness Vickers value of the MDFed CP Ti. (measured on the ND plane).

Lot	A	B	C
Maximum	511	474	435
Average	471	447	398
Minimum	423	417	361

Then the applied stress amplitude in Fig. 12 is normalized by micro Vickers hardness in S-N diagram, as shown in Fig. 13. A similar S-N curve of each lot was obtained, and the difference of fatigue strengths among the lots became smaller, indicating that scatter shown in Fig. 12 could be attributed to the different hardness. All lots have the same fatigue behavior when the different hardness was taken into account.

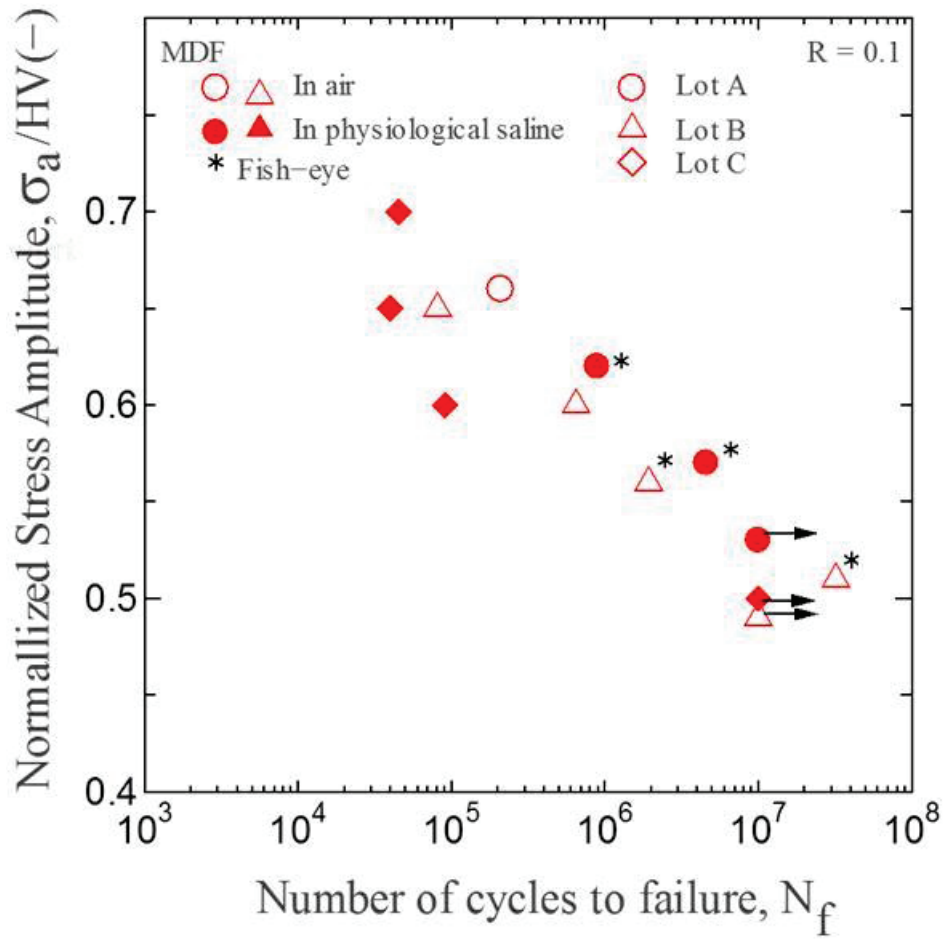


Fig. 13. Normalized S-N diagram of the MDFed CP Ti by Vickers hardness.

2.3.3. Fractography

Fig. 14 shows the typical fatigue fracture surface and magnified view at the crack initiation site of TP35C. Fatigue crack initiated at the corner of the plate, and flat feature at the crack initiation site indicates that cyclic slip deformation resulted in the crack initiation. This surface fatigue crack initiation and propagation mechanisms are typical in many metals. As shown in Fig. 14, the specimen surface near the corner edges are slightly curved by the polishing process of the surface

before fatigue test. But as shown by the scale bar in Fig. 14(a), the change of the cross sectional shape is quite small, because the width of the specimen is 14.9 mm. Thus, it is reasonable to consider that the macroscopic cross sectional shape is rectangular.

Fig. 15 shows the fatigue fracture surfaces of MDFed Ti, where the crack initiation site is indicated by the arrow in the figure. The fatigue crack initiated on the surface of MDFed Ti similar to TP35C. However, sub-surface crack initiation with fish eye was sometimes recognized in MDFed Ti as shown in Fig. 16. In general, sub-surface crack initiation is typically seen in HCF fracture of high strength steels [25, 26] or surface treated alloys, such as DLC-coated magnesium alloy [27] or ultrasonic shot-peened β -type Ti alloy [28]. But sub-surface crack initiation was hardly reported in pure Ti, thus it means that the present case is quite unique phenomena for MDFed Ti.

In Figs. 12 and 13, sub-surface crack initiation was denoted by the asterisk marks “*”. It should be noted that sub-surface crack initiation occurred in the HCF regime, where the number of cycles to failure was longer than 10^6 cycles. At the stress amplitude, σ_a , of 240 MPa, the fatigue test run out at 10^7 cycles in air, which could be defined as fatigue limit. The fatigue test at 240 MPa was then continued until final fracture. Consequently, fatigue fracture occurred at 3.20×10^7 cycles (very high cycle fatigue (VHCF) regime) with sub-surface crack initiation with fish eye (Fig. 16). It indicates that sub-surface fatigue crack initiation occurs in HCF and VHCF regimes. The other emphasis is that sub-surface crack initiation occurred even in Ringer’s solution. Fig. 17 shows the sub-surface crack initiation in Ringer’s solution. If the corrosive environment degrades fatigue properties, surface crack initiation

must dominate fatigue fracture in HCF regime because corrosion occurs on the specimen surface. Therefore, sub-surface crack initiation in Ringer's solution also proves the high corrosion fatigue resistance of MDFed CP Ti.

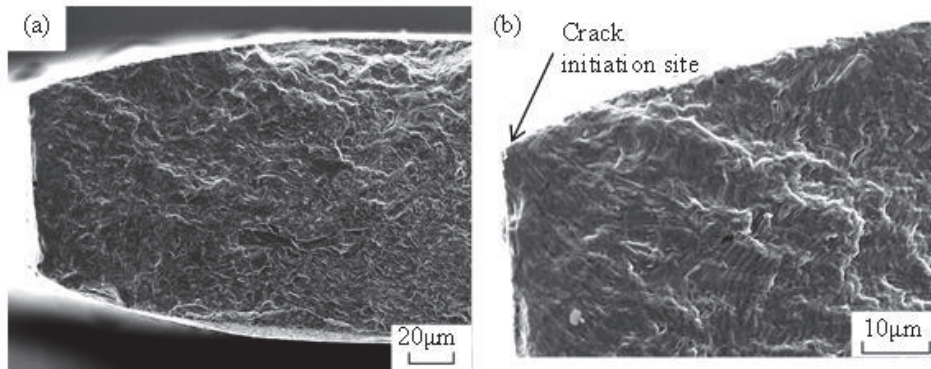


Fig.14. Fatigue fracture surfaces of TP35C: (a) Overview, (b) Magnified view at the crack initiation site ($\sigma_a = 190\text{MPa}$, $N_f = 1.4 \times 10^6$).

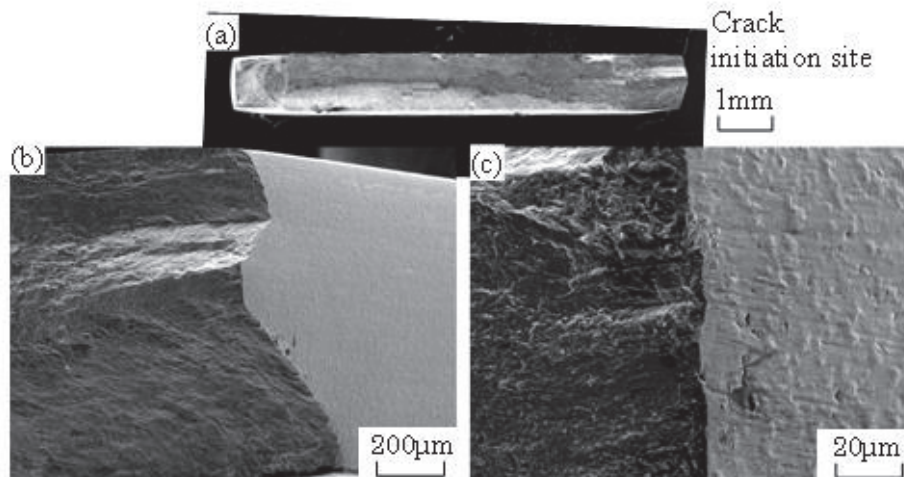


Fig.15. Fatigue fracture surfaces of MDFed Ti in laboratory air (Surface crack initiation): (a) Overview, (b) and (c) Magnified views at the crack initiation site ($\sigma_a = 270\text{MPa}$, $N_f = 6.5 \times 10^5$, Lot B).

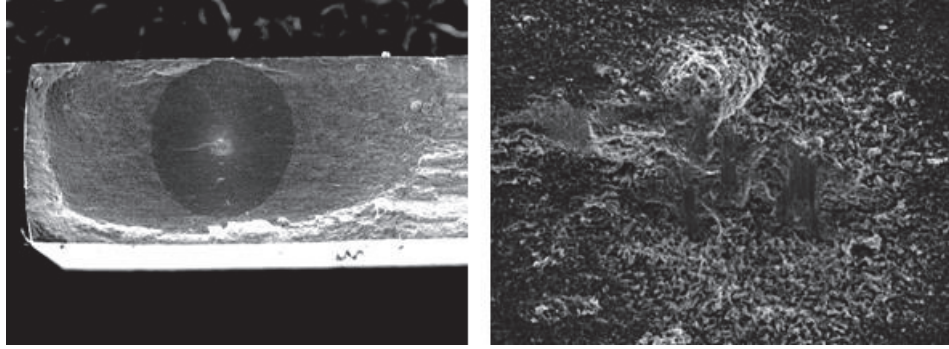


Fig.16. Fatigue fracture surfaces of MDFed Ti in laboratory air (Sub-surface crack initiation): (a) Overview, (b) Magnified views at the crack initiation site ($\sigma_a = 230\text{MPa}$, $N_f = 3.2 \times 10^7$, Lot B).

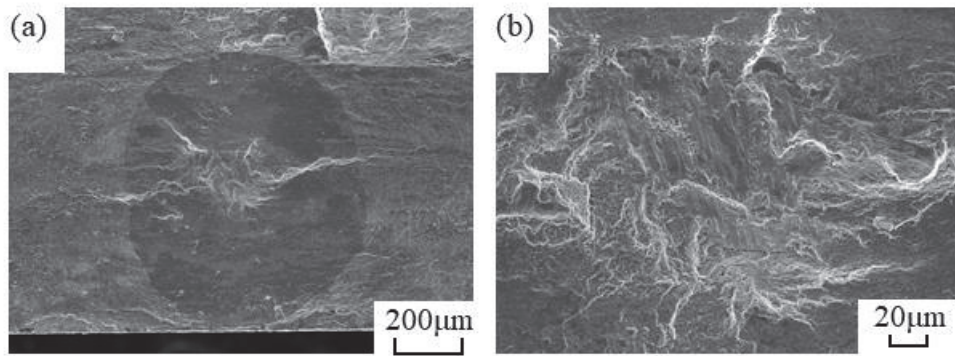


Fig.17. Fatigue fracture surfaces of MDFed Ti in Ringer's solution air (Sub-surface crack initiation): (a) Overview, (b) Magnified views at the crack initiation site ($\sigma_a = 230\text{MPa}$, $N_f = 8.9 \times 10^6$, Lot A).

2.4. Discussion

2.4.1. *Effect of saline environment*

As shown in Fig 12, irrespective of fatigue testing environment, S-N curves of all lots of the MDFed CP Ti are higher than that of TP35C. It indicates that ultrafine grains through MDFing (Fig 7) provide the higher fatigue strength than TP35C with the micron scale grains (Fig 8). On the other hand, the fatigue test at both in laboratory air and in Ringer's solution at lot A of the MDFed CP Ti showed almost one curve. Else, different fatigue strengths among the lots may be related to their hardness (Table 2). It might be well confirmed with Lot C that the lowest curve among them. Only one specimen that fatigue crack initiated from the surface presented some defect on the side surface (Fig 15), but it is not affected by corrosive environment. Therefore, there is no remarkable effect of corrosive environment simulating human body on the fatigue strength or fatigue fracture appearance. It is considered that effect of corrosive environment in human body is negligible for MDFed CP Ti.

2.4.2. *Fatigue mechanism*

As shown in Fig. 7 and Fig. 8, MDFed CP Ti exhibits ultrafine grains while TP35C with the micron scale grains through conventional cold rolling process.

Fractographic analyses showed that fatigue crack initiated at the specimen surface (for all the TP35C or low cycle fatigue (LCF) regime of the MDFed CP Ti) and at the subsurface showing fish-eye in the case of HCF and VHCF the MDFed CP Ti. Heinz reported that sub-surface crack initiation with fish-eye was seen in the VHCF regime of Ti-6Al-4V, while surface failure occurred in the HCF regime [11]. In Ti-6Al-4V alloy, sub-surface crack initiation had been reported in HCF regime [29-31]. Oguma et al. concluded that sub-surface crack initiation occurred due to the cleavage fracture of α -phase in $\alpha+\beta$ microstructure [29]. Therefore, sub-surface crack initiation could be attributed to the inhomogeneous $\alpha+\beta$ microstructure of Ti-6Al-V alloy. However, the microstructure of MDFed Ti consists only of homogeneous α -phases. The sub-surface crack initiation has not been reported for pure Ti. Thus, the sub-surface crack initiation mechanism in MDFed Ti is investigated in detail as follows.

In the high strength steels, inclusions such as intermetallic compound (IMC) and oxide with the size of dozens μm are generally recognized at the sub-surface crack initiation sites [25, 26]. It indicates that inclusions dominate sub-surface crack initiation mechanism. Thus, the sub-surface crack initiation site, namely the center of the fish-eye was analyzed by EDS to identify IMC. Fig. 18 indicates the magnified view at the sub-surface crack initiation site and Ti mapping. Fig. 18(a) is the matching fracture surface of Fig. 16(b), namely the other side of the fracture surface. The spectrum of EDS is also shown in the figure. Only Ti was detected at the center of fish eye, indicating that the sub-surface crack initiation could not be related to inclusions, but to the other microstructural factor.

Subsequently EBSD analysis was conducted near the center of fish eye of Fig 17(a). It is impossible to apply EBSD analysis directly on the rough fatigue fracture

surface. Thus, the fracture surface was polished by emery paper with the depth about 20 μm and then ion milled to get mirror surface. Subsequently, EBSD was performed and the SEM image and inverse pole figure are shown in Fig. 18. The EBSD analysis was conducted in the rectangular area in Fig. 18(a). The area, where Confidence Index (CI) value was lower than 0.1, is shown in black in Fig. 18(b). The MDFed Ti was severely deformed, thus most area is covered by black with low CI values. However, it should be noted that some grains with the size larger than 1 μm are detected. The average grain size obtained from TEM observation was 200 nm as shown in Fig. 7. The Fig. 18 indicates that grain size inhomogeneity exists in the material. The grain size distribution is also shown in Fig. 18(c) in terms of area fraction. When EBSD analyses were conducted on the specimen surface, clear Kikuchi bands were not obtained at all, thus the analytical result was shown only by black area with low CI values. However, some coarser grains are detected near the mid thickness of the MDFed Ti plates as shown in Fig. 18. The other fish-eye fracture surface is shown in Fig. 19. As shown in Figs. 16(a), 17(a) and 19(a), sub-surface cracks predominantly initiated near the mid thickness of the plates. It is considered that sub-surface cracks initiated at coarse grains near the mid thickness. Consequently, it could be concluded that the inhomogeneity of grain sizes near the mid thickness of the plates resulted in the sub-surface crack initiation. As mentioned above, clear Kikuchi bands were not obtained on the specimen surface. Therefore, it is considered that the microstructure is homogeneous on the specimen surface, but inhomogeneity exists near the mid thickness.

It is summarized that the mechanical and fatigue properties of the MDFed Ti plates were superior to those of TP35C plates due to much finer grains. Oguma et al.

conducted fatigue tests using Ti-6Al-4V at the stress ratio, $R = 0.1$, which was the same with the present case [29]. They concluded that the fatigue limit stress amplitude was 225-248 MPa. In the present paper, the fatigue limits are 250 and 220 MPa for the lots A and B, respectively. It could be concluded that combined process of MDFing and rolling of commercial purity grade 2 Ti derives drastic improvement of fatigue strengths comparable to Ti-6Al-4V. Furthermore, no degradation of fatigue properties occurred in Ringer's solution, indicating good applicability of the MDFed Ti plates as medical implants. Unique sub-surface crack initiation was recognized in

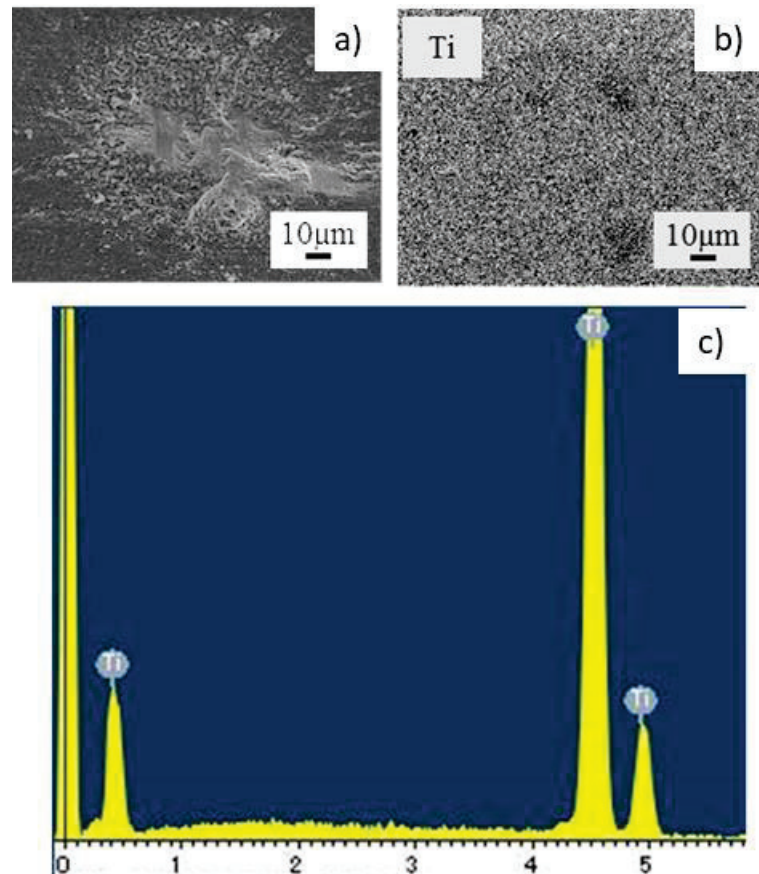


Fig.18. EDS analysis result: (a) SEM image of sub-surface crack initiation site, (b) Ti mapping, (c) EDS spectrum ($\sigma_a = 230\text{MPa}$, $N_f = 3.2 \times 10^7$, Lot B).

the HCF and VHCF regimes of the MDFed Ti plates, which could be attributed to the grain size inhomogeneity.

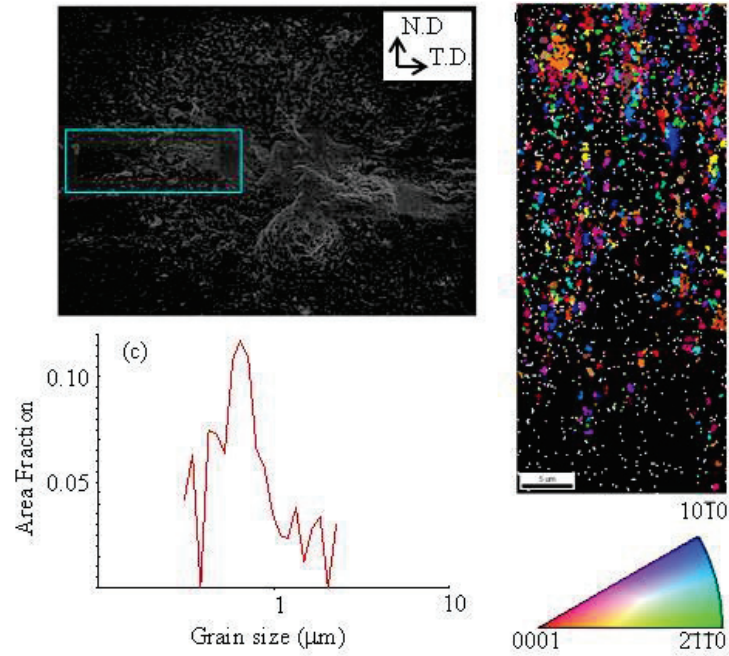


Fig.19. EBSD analysis result: (a) SEM image of sub-surface crack initiation site, (b) Pole figure of the rectangular area in Fig. (a), (c) Distribution of grain sizes ($\sigma_a = 230\text{MPa}$, $N_f = 3.2 \times 10^7$, Lot B).

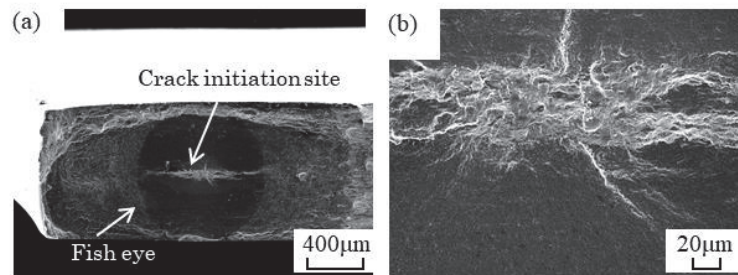


Fig.20. Fatigue fracture surfaces of MDFed Ti in laboratory air (Sub-surface crack initiation): (a) Overview, (b) Magnified views at the crack initiation site ($\sigma_a = 250\text{MPa}$, $N_f = 1.9 \times 10^6$, Lot B).

2.5. Conclusions

Tension-tension fatigue tests were conducted using commercial purity grade 2 Ti thin plates with the thickness of 1 mm fabricated by a combined process of multi-directional forging (MDFing) and rolling (simply referred as MDFing) in air and in Ringer's solution. As comparison, a TP35C produced by conventional cold rolling process was used. Based on the experimental observations, the following conclusions can be made:

1. Both tensile strengths and ductility were drastically improved by MDFing compared to TP35C.
2. Microstructural observation revealed that the average grain size of the MDFed CP Ti plate was 200 nm, while the microstructure of TP35C was a mixture of fine and coarse grain colonies. The size of the coarse grain was about 30 μm . EBSD and XRD analyses revealed that similar textures were formed in both MDFed CP Ti and TP35C.
3. Fatigue strengths of the MDFed CP Ti plates were also higher than those of TP35C. The higher tensile and fatigue strengths of the MDFed CP Ti plates could be attributed to the ultrafine-grained micro structure evolved by MDFing.
4. There is no degradation of fatigue properties of the MDFed CP Ti in the corrosive environment simulating human body.

5. Scatter in fatigue strengths among the different lots of MDFed CP Ti could be related to their different hardness. Higher hardness provides slightly higher fatigue strength.
6. Fatigue crack typically initiated from the surface, exceptionally subsurface crack initiation with fish eye occurred in the MDFed CP Ti plates in the HCF and VHCF regimes, where number of cycles to failure was longer than 10^5 cycles. Microstructural observation proves that inclusion were not at the sub-surface crack initiation site.
7. EBSD analyses revealed that microstructural inhomogeneity with some coarse grains with the size of a few μm existed in the inner part of the MDFed CPTi plate, and the microstructural inhomogeneity resulted in the subsurface crack initiation.

Chapter 3 Effect of Thickness on Tensile and Fatigue Properties of Multi-Directionally Forged Commercial Purity Grade 2 Ti Thin Films

Abstract

The tensile properties and fatigue behavior of commercially pure titanium CP Ti grade 2 thin foils which were fabricated by multi directional forging (MDFing) were investigated in the laboratory air. The thin foils were developed for using in bio implant application. The thin foils have four different thicknesses; namely 13, 20, 30 and 50 μ m. Compared to the thin plate of 1 mm in thickness, there is no big difference in the tensile and fatigue strengths, but elongation gradually decreases along more thinly foils. It seems that there is no effect of thickness on tensile and fatigue strengths of MDFed CP Ti grade 2 thin foils. Fracture surface observation showed that only surface crack initiation occurred and distinguishable final fracture feature was in the shape of flat or slant depending on the film thickness. In the unstable crack propagation area, abundant dimples appeared on thicker foils, while dimple-area was limited in 20 μ m then almost disappear on 13 μ m foil thickness. Less in thickness means less or zero of internal defects as the source of dimples. The less internal defects could be related to the high tensile and fatigue strengths of MDFed CP Ti grade 2 thin foil.

Keywords: MDFed CP Ti grade 2, thin foil, fatigue strength, foil thickness, dimples, final fracture.

3.1 Introduction

In recent years, Ti and Ti alloys are widely used in many applications due to many attractive attributes such as low density, high stiffness and strength-to-weight ratio, adaptability to low temperature, excellent corrosion resistance, and excellent compatibility with human soft tissue [32-35]. Their excellent strength-to-weight ratios and providing weight savings are attractive to the aerospace and petrochemical industries; high corrosion resistance are needed in the aerospace, chemical, petrochemical and architectural industries; adaptive on both elevated and cryogenic temperature are required for aerospace and chemical industry; and biological compatibility is the most interest to medical care industry.

Corrosion resistance is one of the major features of Ti and Ti alloys. Ti alloys have excellent corrosion resistance against seawater as same as platinum. A strong resistance to corrosion is continuous uniform passive film of Ti oxides over surface. Even when this film is damaged, matrix of Ti will be re-oxidized by contact with air. However, this oxidized Ti is a kind of passivity film that prevents further oxidation.

Another big advantage of Ti and Ti alloys is low density; only about 56% of

stainless steel, and relatively high strength; pure Ti has a tensile strength of 275 ~ 590MPa. Comparing tensile strength with density is known as strength-to-weight ratio or specific strength. Those quantitative data imply that only about a half in weight of stainless steel, when Ti used as structural material. It can be said that Ti and Ti alloys are in a top class in the non-ferrous metal.

Most popular materials among Ti and its alloys for biomedical application are commercially pure titanium (CP Ti) and Ti-6Al -4V. The CP Ti has 4 different grades, in which higher grade has higher mechanical strength with lower elongation at failure. Ti-6Al -4V is considered as grade 5 [18]. These varying properties might be raised by interstitial elements (C, O, N), and alloying elements (Fe, Al and V).

Higher grade also means higher content of impurities. In Ti-6Al -4V, Al and V are required for high strength but unfavorable for bio-integration. There are some allergic cases related to impurities content in implant metal, specifically Al and V [36]. Therefore, CP Ti with fewer impurities but with a high mechanical strength is the most favorable to be used in biomedical application. Furthermore, the strengthening methods without adding any impurities or alloying are desired.

That can be accommodated with refining microstructure through applying severe plastic deformation (SPD) on the subjected material. The main concept of

SPD is giving a massive strain and severe deformation on the material without changing the geometry of material itself. It will result in a significant decreasing of grain size from several hundred micron into submicron or nano scale.

The SPD on titanium and titanium alloys could be done by Equal Channel Angular Pressing (ECAP) [37], Accumulative Roll Bending (ARB) [38], High Pressure Torsion (HPT) [39] and Multi Directional Forging (MDF) [40]. Among the SPD methods, MDF, as shown in Fig. 21, is quite easier to be applied for industrial application and most applicable to be used in bulk size material. Mathematically, a high strain of about 0.8 is successfully introduced on the subjected material by 1 pass of consecutive forging at all orthogonal direction X, Y and Z. Our collaborator researcher, Prof. Miura had succeeded to increase the strength of CP Ti up to 960 MPa with elongation at failure of 18%. MDF on CP Ti is promising with a big change in mechanical strength without loss in ductility.

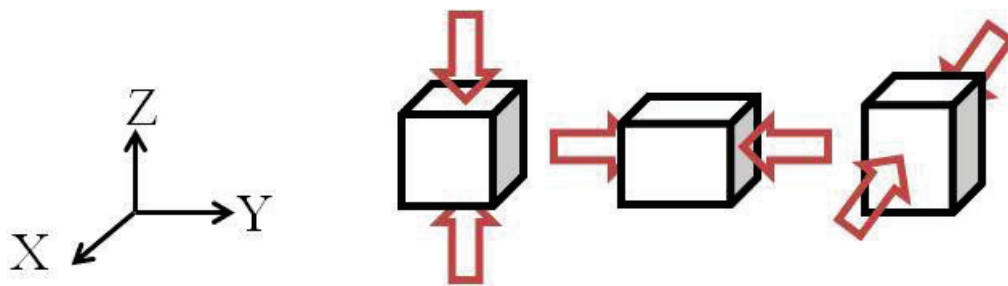


Fig. 21. Mechanism of MDF.

Fatigue behavior of CP Ti produced by MDF should be well understood prior to long-term use as structural components, mainly biomedical application. Mg alloys and Al alloys which were well explored by MDF and fatigue, but there is still a limited number report of MDF and fatigue on Ti and its alloys. Therefore, fatigue behavior of CP Ti thin foil, which were fabricated by Multi-Directional Forging, was investigated. Tensile properties were also studied to confirm the fatigue behavior. Some fatigue crack propagation (FCP) tests are also conducted.

3.2 Experimental Details

3.2.1. Materials

The materials used in this study are CP Ti grade 2 produced by MDF. There are four thin foils with different thicknesses (13, 20, 30 and 50 μ m). The physical appearances of thin foils could be seen in Fig. 22. For reference a CP Ti grade 2 thin plate of 1 mm in thickness was also used in this study. The details of the reference plate are described in the previous chapter. All the material was supplied from Kawamoto Heavy Industry.

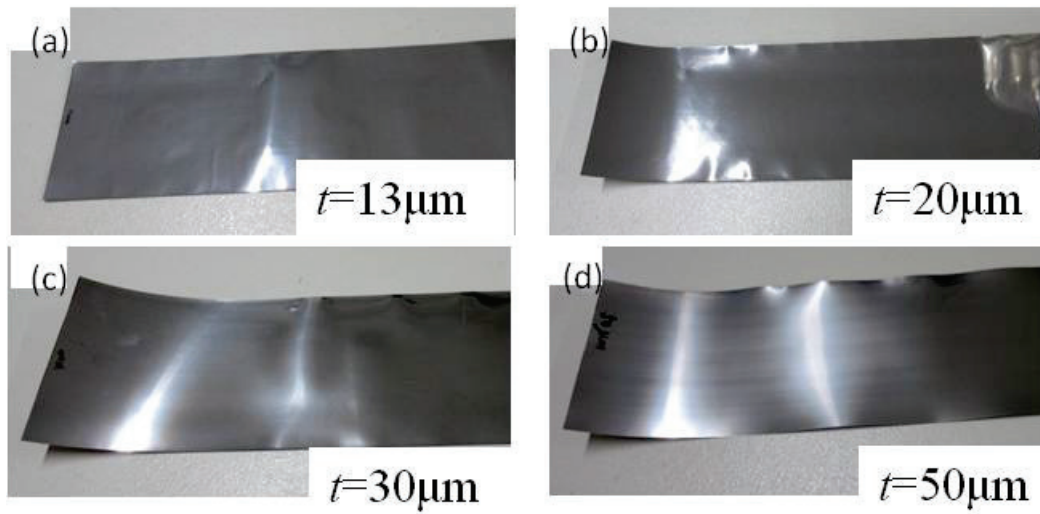


Fig. 22. As-received material of CP Ti thin foil grade 2 fabricated by MDF, supplied from Kawamoto Heavy Industry.

3.2.2. Specimens and procedures

Two kinds of tests were conducted i.e. tensile and fatigue tests. Specimen blanks for these tests were cut off from the as-received foils in rolling direction (RD). The specimen geometries for both tensile and fatigue tests are shown in Fig. 23. The specimen for tensile test has a width of 5 mm, total length of 37 mm, and gage area of 6 x 1.4 mm (gage length-width). And the specimen for fatigue test has dimension; width of 5 mm, length of 23.1 mm, an outside semicircular notch with radius of 15mm, and a minimum width in gauge length of 2 mm.

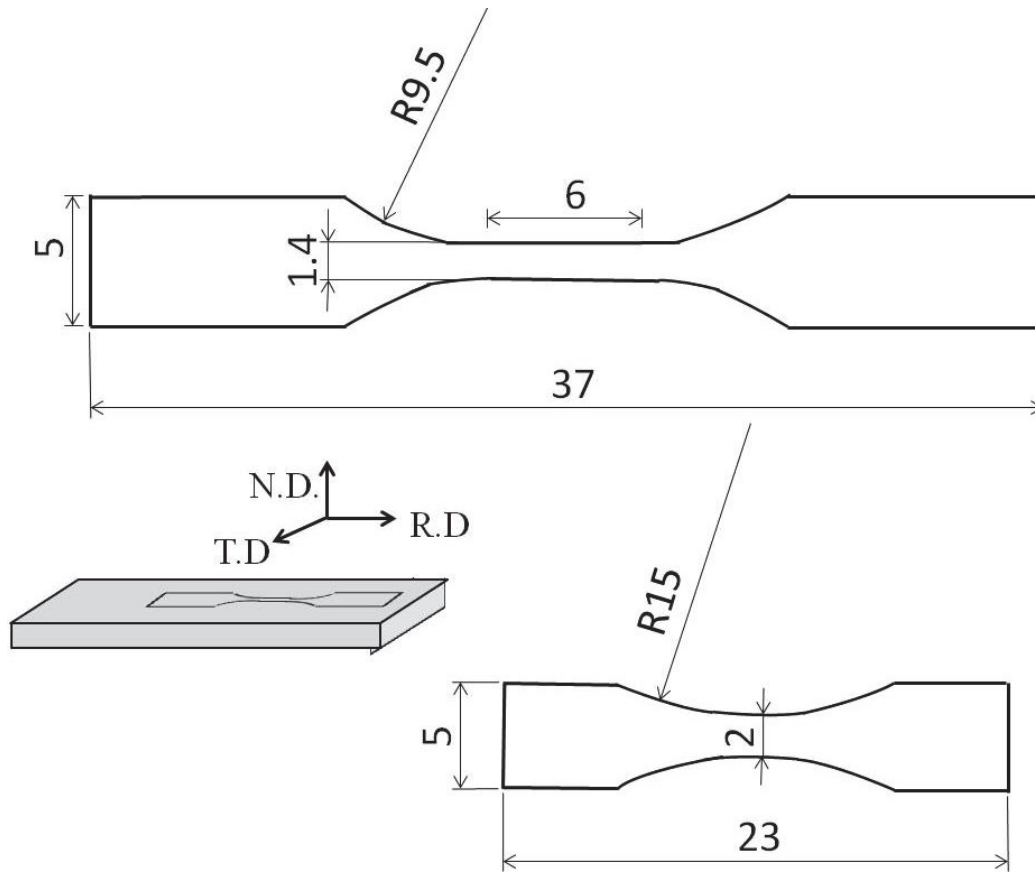


Fig. 23. Specimen geometry of;(up) tensile test, (bottom) fatigue test.

The followings are specimen preparation procedures. First, the blank was hold between two jigs and fastened by bolt-nut system as shown in Fig. 24. Then, the blank was wet-polished along rolling direction with abrasive paper up to #2000, followed with the polishing by alumina paste and diamond suspension of 1 μm . The result of polishing was a mirror-like surface. Specimen was finished with ultrasonic cleaner in alcohol solution, and cold-hair drying.

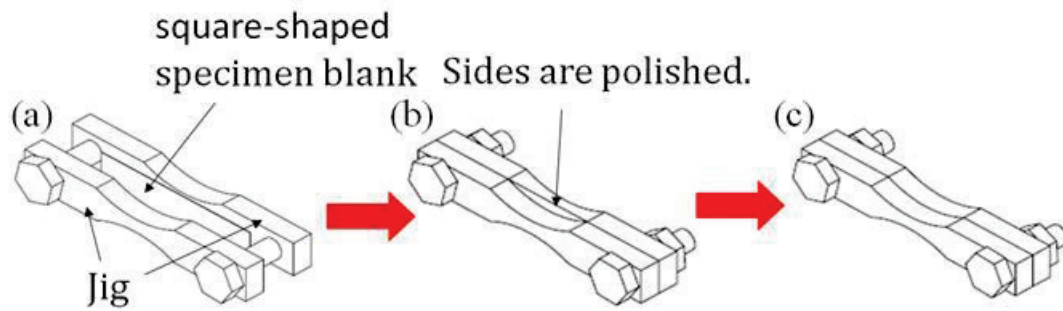


Fig. 24. Specimen preparation for tensile and fatigue test.

Both of the tensile and fatigue tests were conducted using Shimadzu MMT-100N air-servo machine in laboratory air. The tensile tests were conducted under displacement control with a displacement rate of 1 mm/min. Parallel length of the specimen was black marked with oil pen. Both of ends of the tensile specimen were glued with an instant adhesive on cross heads, and hold with bolt-clamp, as shown in Fig. 25. Changes of load and cross head displacement on controller display were recorded by camera video. By that, force and cross head displacement curve was constructed by a simple computational method.

The sinusoidal fatigue tests were done with a stress ratio, R of 0.1 and a frequency of 20Hz. Specimen treatment and positioning are the same with the tensile test. The test was finished when specimen broke or run-out at 107 cycles. The fracture surface of the specimen was examined using a scanning electron

microscope (SEM).

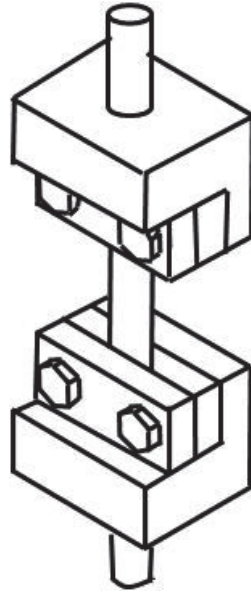


Fig. 25. Set up specimen for tensile and fatigue test.

3.2.3. Fatigue crack propagation (FCP) test

In order to understand the fatigue mechanism of MDFed CP Ti, a FCP test was conducted on thickness of 13 and 50 mm, the thinnest and thickest material. Simple fatigue specimen was prepared with dimension width of 20 mm and length of 44 mm, as shown in Fig. 26. In the middle of specimen, a notch was fabricated by a cutter as a crack starter. A thick line of oil pen was introduced across the crack starter to help in crack propagation observation.

Specimen set up on MMT-100N machine as same as tensile and fatigue tests shown in Fig. 25. The Loading ratio, R was kept on 0.1. FCP test was conducted at

frequency of 20 Hz. By applying a certain tension stress, the starter notch will be developed into a new crack, known as pre-cracking. The effect of cutter was assumed annihilated with this pre-crack development, in this case crack had been developed about 1 mm, and then FCP test was started.

Propagation of the crack was observed by travelling microscope which was placed next to FCP specimen that installed on the MMT-100N machine as shown in the Fig. 25. At the beginning of FCP test, stress intensity factor range, ΔK was lower than in pre-cracking process. The ΔK will be increase by keeping applied stress constant during FCP. The interval between crack observations was adjusted with the

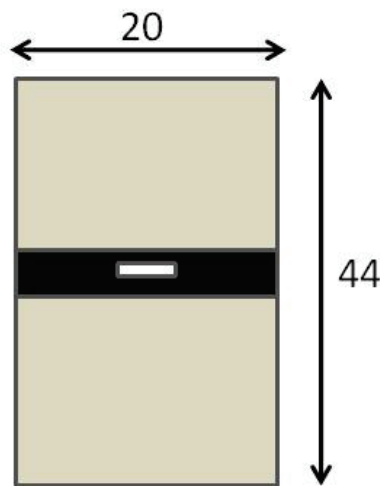


Fig. 26. Specimen appearance for FCP test.

crack progress. Basically, crack increment between two observations is about 0.01 – 0.05mm. Every time of the observation, test was interrupted by reducing the

frequency of FCP to 0.5 Hz to enable the crack length measurement. After measurement was finished, frequency was back reset to 20 Hz.

Because the specimen is treated as center cracked plate tension specimen (CCT), the mathematic formula of CCT specimen which is proposed by H. Tada in the Stress Intensity Factor Handbook Vol. 1 page 3, could be applicable. The stress intensity factor, K_I is defined as

$$K_I = \sigma \cdot \sqrt{\pi \cdot a} \cdot F_I^*(\alpha)$$

whereas σ is applied stress, a is half of crack length, α is ratio of crack length-to-width of specimen.

$$\alpha = \frac{2a}{w}$$

then $F_I^*(\alpha)$ is defined.

$$F_I^*(\alpha) = (1 - 0.025\alpha^2 + 0.06\alpha^4)F_I(\alpha)$$

$$F_I(\alpha) = \sqrt{\sec\left(\frac{\alpha \cdot \pi}{2}\right)}$$

Because of $R > 0$, then $\Delta K = (1-R) K_{max}$, so in this case stress intensity factor range,

Δk is defined as

$$\Delta K = 0.9\sigma_{max}\sqrt{\pi \cdot a} \cdot F_I^*(\alpha)$$

3.3. Results

3.3.1. Tensile properties

A typical load and cross head displacement curve in tensile test is shown in Fig. 27. This figure showed that the specimen with the thickness of 50 μm , and provides a maximum stress of 828 MPa and a maximum elongation of 15%. These values seem not to be so big different from the specimen thickness of 1 mm, whose tensile strength and elongation are 920 MPa and 18%, respectively. All the tensile properties of thin foils are summarized in Table 3. The decrease in thickness of specimen made reduction of elongation of specimen in a countable degree. That was found that all specimens broke a few seconds after maximum stress. But tensile strengths were in the range of 828~1050 MPa, and higher than that of TP35C in the previous chapter

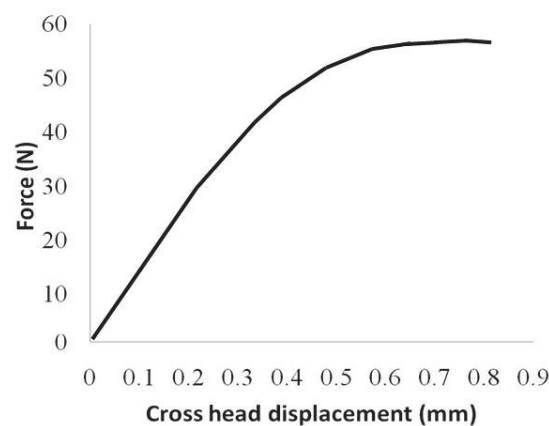


Fig. 27. A typical tensile test curve. Specimen thickness is 50 μm .

Table 3. Tensile properties of MDFed CP Ti thin foil

Thickness, μm	Yield strength σ_y [MPa]	Tensile strength, σ_B [MPa]	Elongation, δ [%]
13	-	1046	8
20	-	933	13
30	-	1050	15
50	-	828	15
1 mm	766	920	18
0.15 mm TP35C	619	746	7

3.3.2. Fatigue Properties.

S-N curves of all the specimens were shown in Fig. 28, in which 107 cycles was set as maximum cycles and 'run-out' criteria. The fatigue limits of all the thicknesses are summarized in Table 4. It shows that the MDF provides higher fatigue limits than the conventional cold rolling process. Value of fatigue limits are 230MPa, 240 MPa, 200 MPa and 220 MPa for the thickness of 50, 30, 20 and 13 μm , respectively. The 50 μm specimen has equal fatigue limit with CP Ti grade 2 thin plate of 1 mm that also fabricated by MDF [41]. Highest fatigue limit was found on specimen with the thickness of 30 μm , but further decrease in thickness of specimen into 20 μm and 13 μm , made the fatigue limit trend become scattering. However, this

scattering is not a large difference among thicknesses. It may indicate that the applied processing after MDF on CP Ti is an adequate process to be applied in producing any variants thickness of foils without altering fatigue life.

Values of mechanical properties and fatigue strengths showed a similar trend. They are scattering with the highest mechanical strengths on the specimen with thickness 30 μ m. When the applied stress amplitudes of fatigue tests are normalized with their mechanical tensile strengths, then normalized S-N curve become closer among the different thicknesses. The normalized stress amplitudes at fatigue limit varied between 0.2-0.3 as shown in Fig. 29.

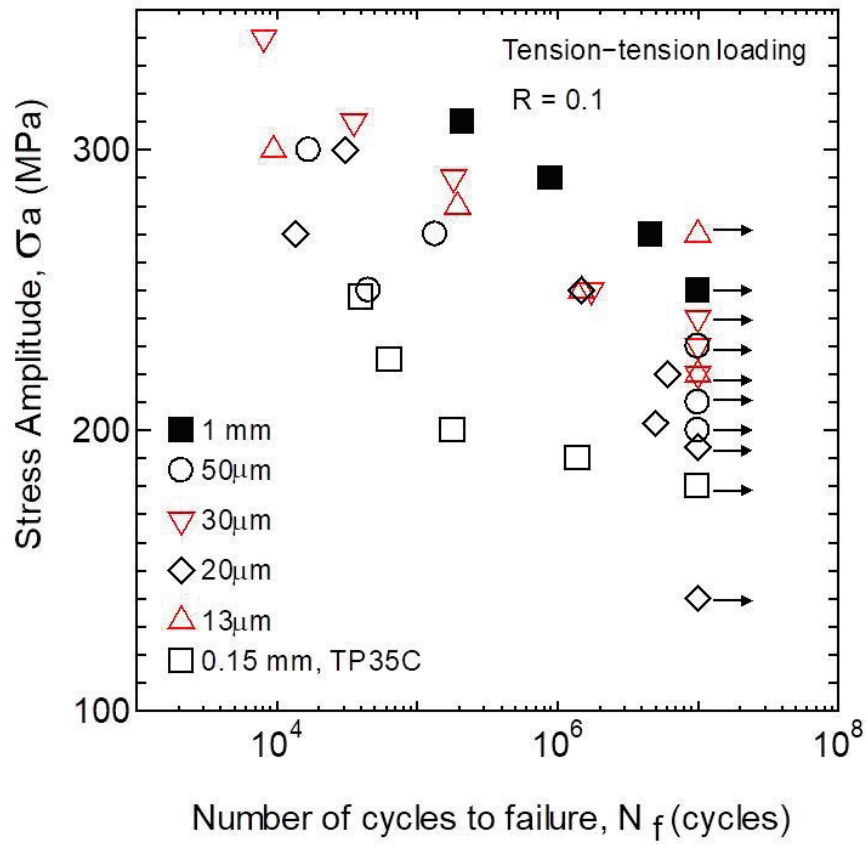


Fig. 28. S-N diagram of CP Ti thin foil fabricated by MDF.

Table 4. Tensile and fatigue strength of MDFed CP Ti thin foil

Thickness, μm	Tensile strength, σ_b [MPa]	Fatigue limit, σ_w [MPa]
13	1046	220
20	933	200
30	1050	240
50	828	230
1 mm	920	250
0.15 mm TP35C	746	180

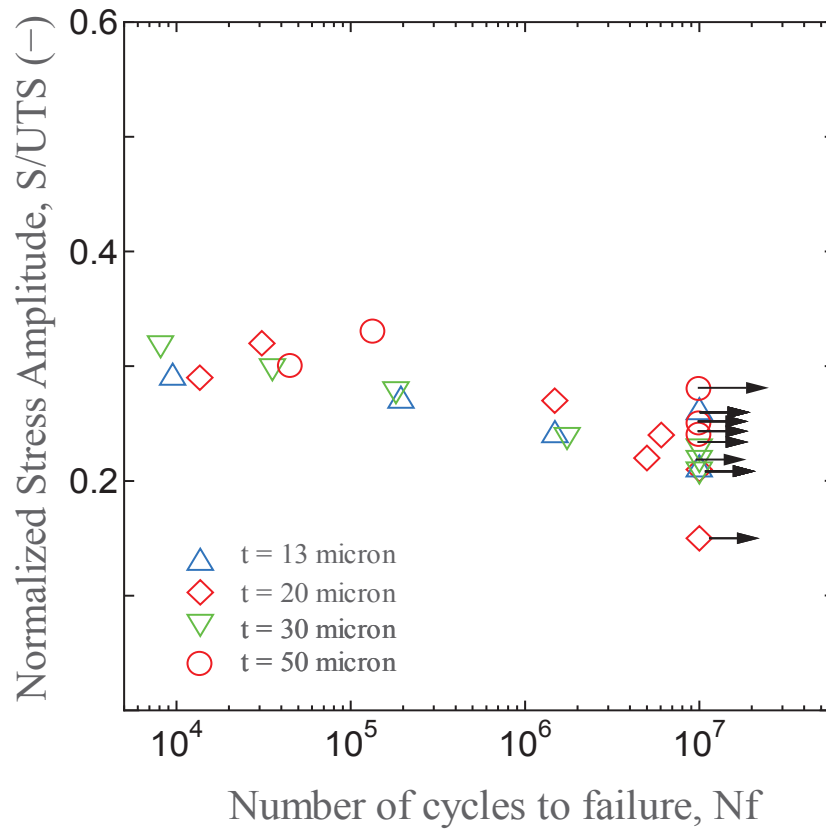


Fig. 29. Normalized S-N diagram of CP Ti thin foil fabricated by MDF.

3.3.3. Fractography

Fracture surfaces of tensile test specimen with thickness of 13 μ m could be seen in Fig. 30. It is a step-like crack from edge of specimen in rectangular B, and a slant exists in the other edge of specimen (in rectangular D). It indicates that crack starts from surface or edge of the specimen in the rectangular B, and propagates to C and catastrophically fractured in rectangular D. No dimples were observed on the surface of the specimen, which might be related to zero internal defect of the

specimen with thickness of $13\mu\text{m}$. The same features were also found on the tensile-fractured test specimen with thickness of $20\mu\text{m}$ as shown in Fig. 31. However, some dimples were revealed during crack propagation area.

Clearer slant was shown on the fracture surface of tensile test specimen with thickness of 30 and $50\mu\text{m}$, which could be seen in Fig. 32 and Fig. 33, respectively. This slant might be promoted by shear stress during the tensile test. That was a feature of many dimples with shear slip along this slant, as showed by Fig. 33c and Fig. 33d. In contrary, there is no dimple in Fig. 33b, which is in a flat fracture. It is considered that crack started from rectangular B, and propagated to rectangular D.

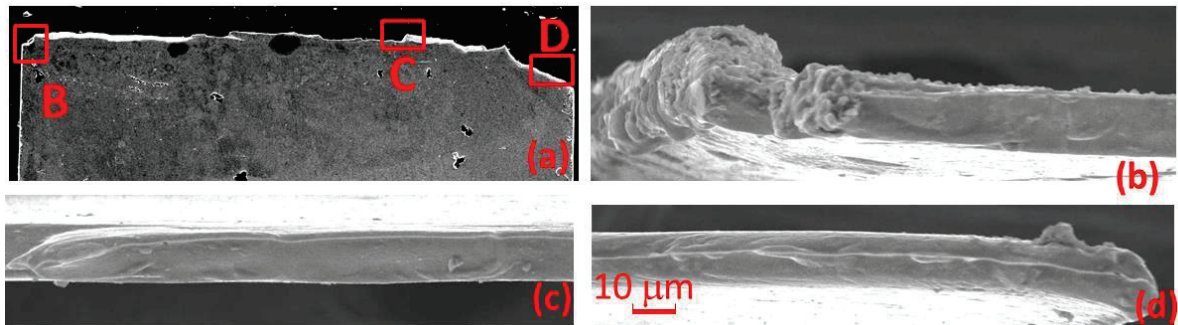


Fig. 30. SEM micrographs showing tensile failure surface of $13\mu\text{m}$ foil specimen, (a) whole view, (b) magnified view at B, (c) magnified view at C, (d) magnified view at D.

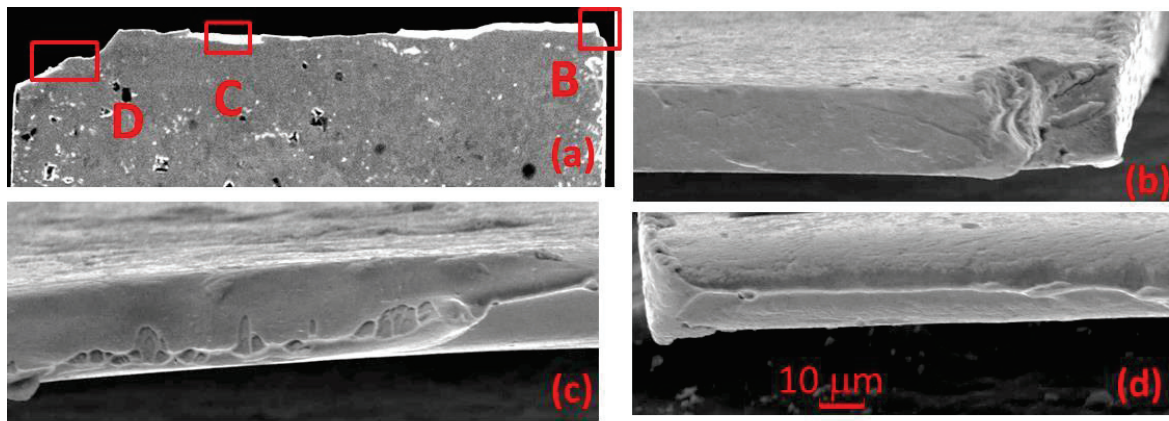


Fig. 31. SEM micrographs showing tensile failure surface of 20 μm foil specimen, (a) whole view, (b) magnified view at B, (c) magnified view at C, (d) magnified view at D.

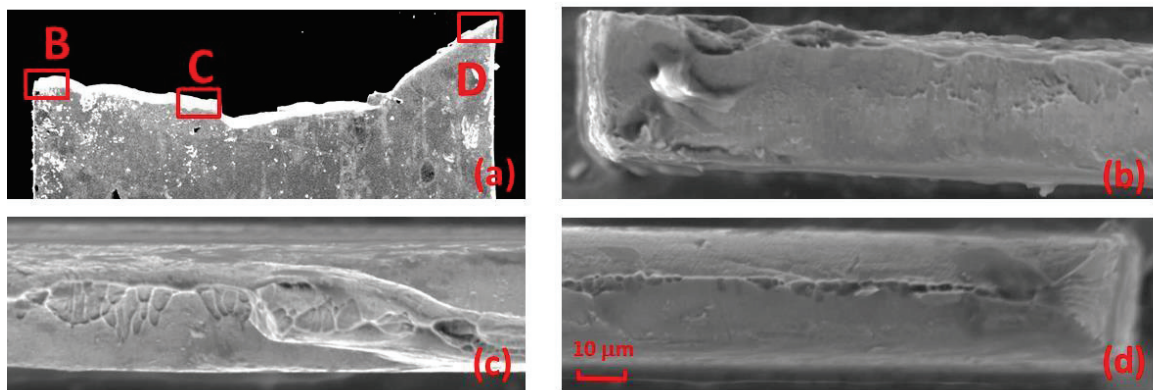


Fig. 32. SEM micrographs showing tensile failure surface of 30 μm foil specimen, (a) whole view, (b) magnified view at B, (c) magnified view at C, (d) magnified view at D.

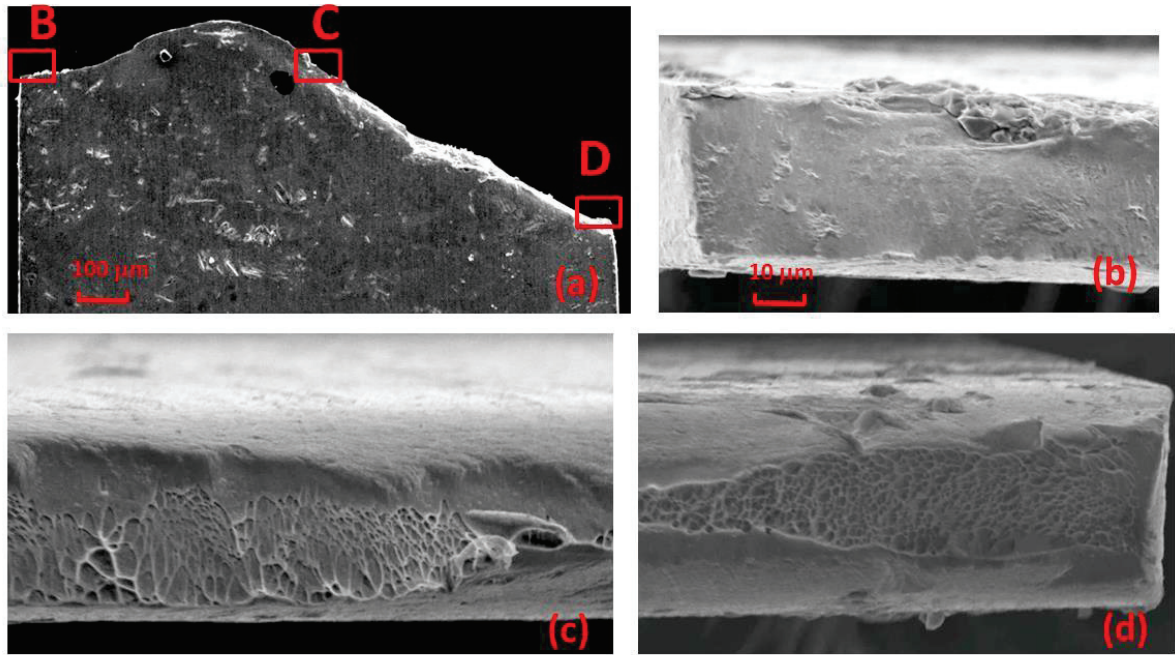


Fig. 33. Fracture surface of tensile test on specimen thickness of 50 μm ; (a) longitudinal crack path, (b,c,d) zoom view at the same magnification of rectangular A,B,C respectively.

In order to understand the fatigue fracture mechanism of MDFed CP Ti grade 2 thin foils, some representative micrographs were presented in the transversal and longitudinal direction. Transversal direction is parallel with width direction of specimen, and longitudinal is in the thickness direction or cross section. First, a fracture surface of MDFed CP Ti thin foil of 13 μm is shown in Fig. 34. Fracture line that travels along width of the specimen is almost horizontal, but there is a slant at the right and left end as shown in Fig. 34.a. Right end (Fig. 34b) showed a rough

surface of slant. Then a line of slant was seemed to be parallel with fracture line (Fig. 34c) and remained in the left end (Fig. 34d). From the appearance, crack started from the right end, then propagated into left direction till final fracture had occurred.

Second, similar features near the edges of fracture surface were also found on the specimen with the thickness 20 μm , except many dimples appeared on the cross section in Fig. 35. The right end of the specimen showed rough feature (Fig. 35b), while reverse end revealed a slant feature (Fig. 35e). Fig. 35c showed a colony of dimples start to appear on rectangular B position. The area between rectangular B and D is characterized with feature of dimples and flat surface as represented in Fig. 35d.

Another type of fatigue fracture surface is horizontal fracture line without slant trace on the surface, and that could be seen in Fig. 36. All broken specimens of 50 μm showed the same feature with Fig. 36. Crack initiated on the left end (Fig. 36b) with feature of rough surface, then crack propagated into right direction. Dimples start to appeared at C rectangular, and remained till specimen broken at the right end (Fig. 36d). The end of the specimen that experienced final fracture showed no sinking of the cross section.

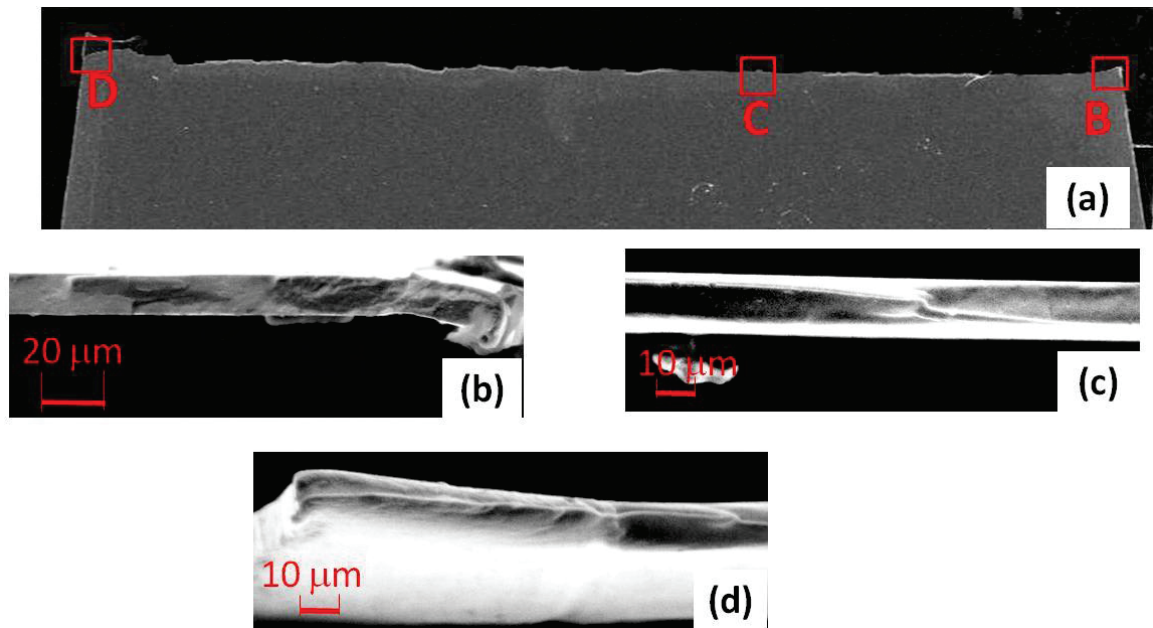


Fig. 34 . SEM micrographs showing fatigue fracture surface of 13 μm foil specimen, $\sigma_a = 250 \text{ MPa}$, $N_f = 1.4 \times 10^6$ cycles; (a) longitudinal fracture line, (b) magnified view at B, (c) magnified view at C, (d) magnified view at D.

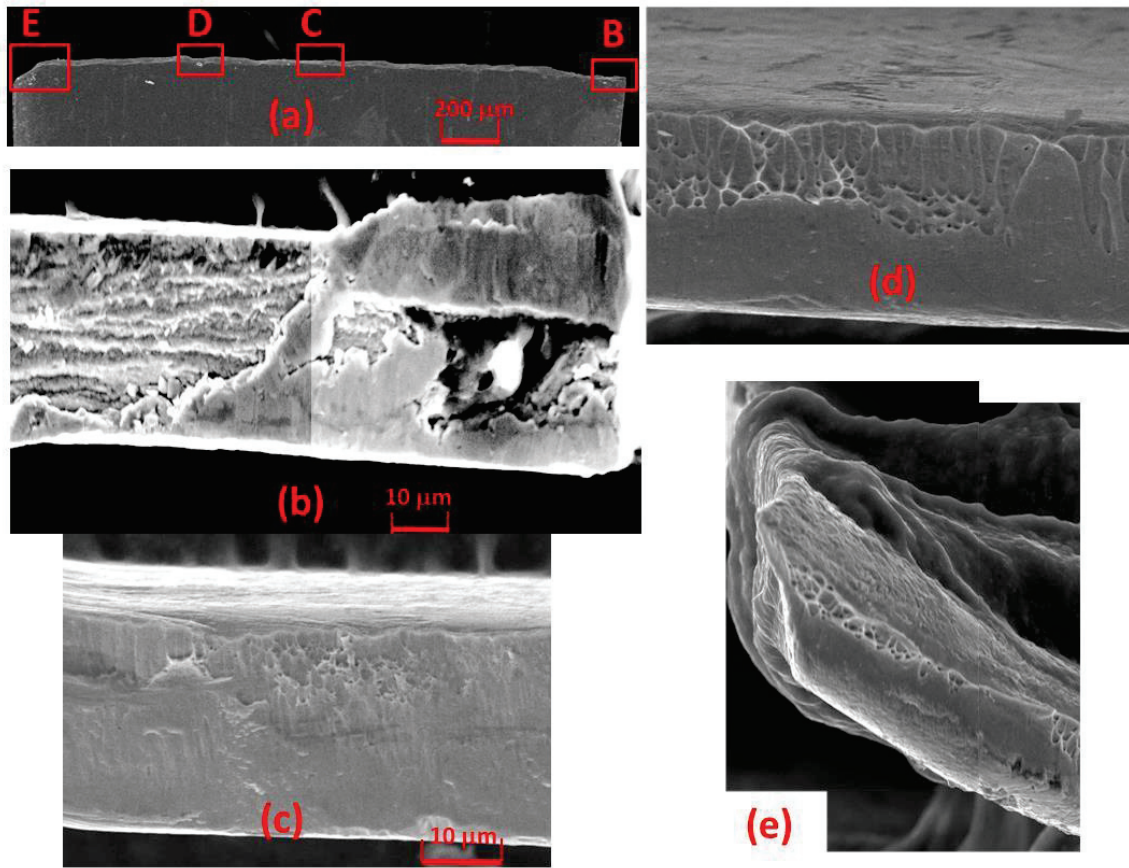


Fig. 35. SEM micrographs showing fatigue fracture of specimen thickness of 30 μm , tested at 290 MPa and broken at 181,602 cycles; (a) longitudinal fracture line, (b-e) zoom view of their capital rectangular.

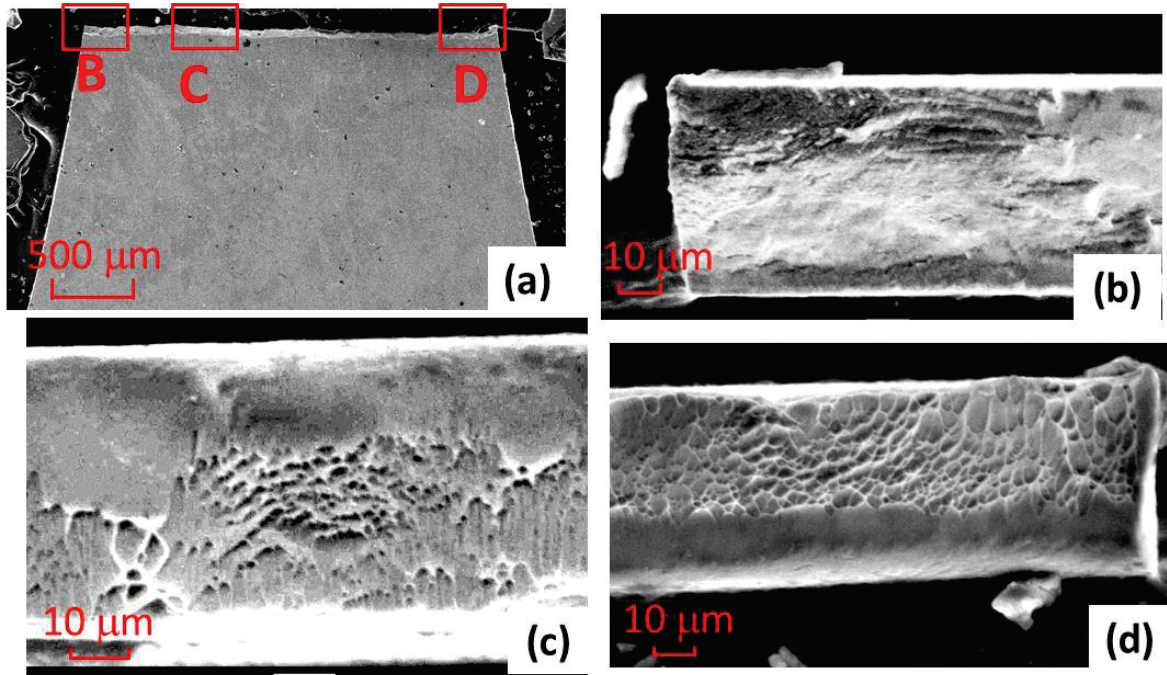


Fig. 36. SEM micrographs showing fatigue fracture surface of 50 μm foil specimen, $\sigma_a = 270 \text{ MPa}$, $N_f = 1.3 \times 10^5$ cycles; (a) longitudinal fracture line, (b) magnified view at B, (c) magnified view at C, (d) magnified view at D

Fatigue crack propagation (FCP) line on the thin foil specimen could be seen in Fig. 37. Crack propagation direction is perpendicular to the loading axis or in smooth horizontal line. This smooth line was also reported by Fintova et. al on ultra-fine grained CP Ti grade 4 [42]. Rough line in the middle of specimen is a cutting trace as an artificial crack starter. Crack was incubated for hundreds thousand cycles, then start to propagate slowly and accelerated with increasing number of cycles, as shown in Fig. 37. Fig. 38 shows crack propagation curve. FCP

rates vs stress intensity factor range curve was shown in Fig. 39. The lowest point of the curve has the FCP rate of $3.89 \cdot 10^{-7}$ mm/cycle with stress intensity factor range, ΔK of 4.53 MPa.m^{1/2}. The extending imaginary line on the curve into FCP rate of 10^{-7} mm/cycle might result in ΔK_{th} value of ~ 4 MPa.m^{1/2}. This value is less than the stress intensity factor threshold of the coarse-grained CP Ti grade 4, but higher than UFG CP Ti grade 4 which was processed by combination of ECAP and cold drawing [42].

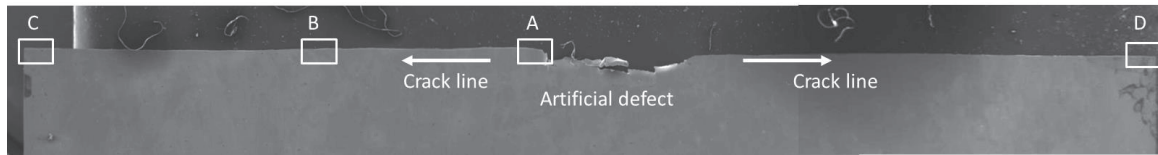


Fig. 37. Typical crack propagation line on FCP test specimen.

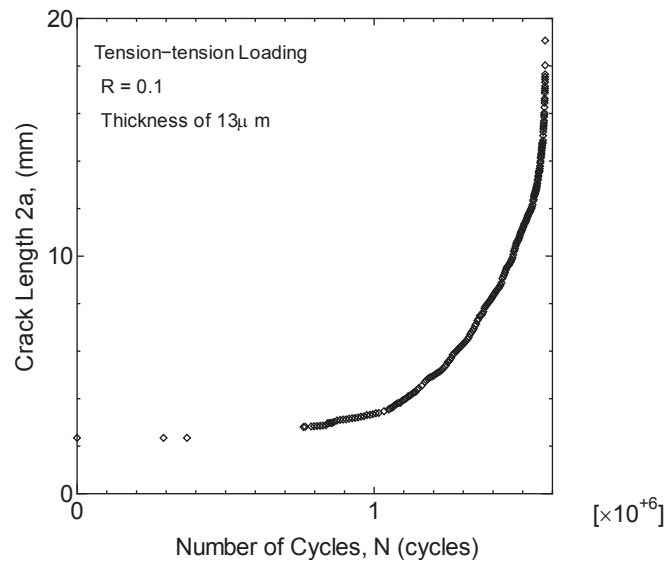


Fig. 38. Typical crack propagation curve, specimen thickness of 13 μ m.

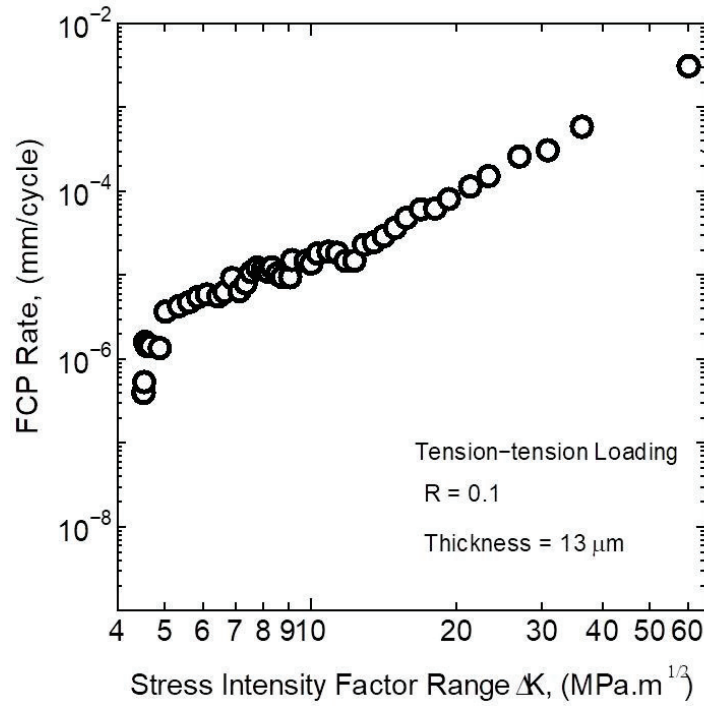


Fig. 39. FCP test result of specimen thickness of 13 μm .

3.4. Discussion

Fabrication of CP Ti thin foil by MDF had increased mechanical and fatigue strengths, with less of ductility loss. Increase in the tensile and fatigue strengths contains scattering among the thicknesses of thin foils, as seen in Table 4. Thickness of 30 μm seemed to have the highest mechanical and fatigue strengths. But, there is no clear relation between thickness and mechanical and fatigue strengths. However, ductility of thin foils gradually decreased with decreasing the thickness. Less thickness provides lower ductility, but still higher than the ductility of conventional rolled TP35C. It may be related to the effect of the process in making thin foils after

MDF. Less in final thickness of thin foil means that higher deformation had applied in the process, which made thin foils be more brittle. Normally, decrease in the thickness made some loss in ductility, which were accompanied with increase in strength, but in our specimen that is not always true. Therefore, the effect of thickness on tensile and fatigue strengths is not clearly seen.

Fig. 35 shows typical examples of fatigue fracture surfaces. Fig. 35a shows the side view of the fatigue-fractured sample with the thickness of 30 μ m. Large plastic deformation or necking is not observed besides the left edge after fatigue tests. Figs. 35b, 35c and 35d correspond to “B”, “C” and “D” in Fig. 35a, respectively. Fig. 35b shows a step-like rough surface in the left half, but comparatively large cleavages and flat surfaces are observed in the right half. Fig. 35c shows a colony of dimples in the upper half and a flat surface in the lower half. This feature is also observed in “D” in Fig. 35a as shown in Fig. 35d. It is considered that a fatigue crack initiated from the right edge since dimples are observed in the left half in the whole fracture surface. In short, fatigue cracks generally initiated at the edges of foils irrespective of foil thicknesses. It indicates that internal defect did not act as crack starter or the internal defect is too few in the interior of the thin foils. It is well confirmed with Fig. 32 that only two or three dimples was found on the fracture

surface.

Another feature of the fatigue fracture is slant at opposite edge, where crack initiation took place. In common sense, slant is formed because of excess massive of shear stress at the end stage of fatigue test. Dimples always present on the cross section surface of the slant. It seems that number of dimples was reduced with decrease in the thickness of foil, and thicker specimen provides higher ductility as seen in Table 3. Hernandez-Rodriguez et al. reported that dimples are a sign of ductility on the fracture surface of Ti alloys [43]. It may be related to higher reduction of the cross section of thin foil. However, less dimples are not always related with higher strength among the thin foils, because the most strongest foils are the thicknesses of 30 and 13 μm .

On the other hand, slant is not always seen on the specimen surface. Slant tends to happen on the specimen with the thickness less than 50 μm , as shown in Table 5. The flat end surface revealed on 50 μm or on 30 μm with the high stress amplitude (250 MPa). This table had characterized features of the final fracture stage. Overall, it seems that there is less or no effect of thickness on the initial fatigue fracture, but may be related to the final fracture mechanism.

Table 5. Condition of last end of MDFed CP Ti grade 2 thin foil after fatigue test.

Thickness (μm)	Applied Stress Amplitude (MPa)									
	310	300	290	280	270	250	240	230	220	200
13	-	F	-	S	-	S	-	-	O	-
20	-	-	-	-	S	S	-	S	S	O
30	S	-	S	-	-	F	O	-	-	-
50	-	F	-	-	F	F	-	O	-	-

Note: - : no test. F: Flattened. S: Slant. O: no fracture, specimen reaches 10^7 cycles, run-out.

In the term of FCP test, fracture surface of the specimen in Fig. 40 was took based on rectangular A, B, C in Fig. 37. Distortion at right end in Fig. 40.a is related to the artificial starter as prepared during specimen preparation. A rough surface was shown next to this artificial starter is caused of high stress intensity factor range applied for pre-cracking process. By progress of cracking, fracture surface of FCP specimen tends to be more flattened plane, as shown in Fig. 40b and Fig. 40c. It is well confirmed with a horizontal crack line as shown in Fig. 37. These features are in good agreement with the report of Fintova et. al. that ultra-fine grained CP Ti grade 4 produces fracture surface with transgranular type [42]. Based on Lütjering and Williams, transgranular fracture type is most preferable in the structure with small

grain size, because of high difficulty of nucleating of cleavage cracks [44]. One edge of the specimen showed a feature of stretching or slant as shown in Fig 40.d. Stretching is a feature of tensile fracture related to insufficient area of material against applied stress at the end of the test.

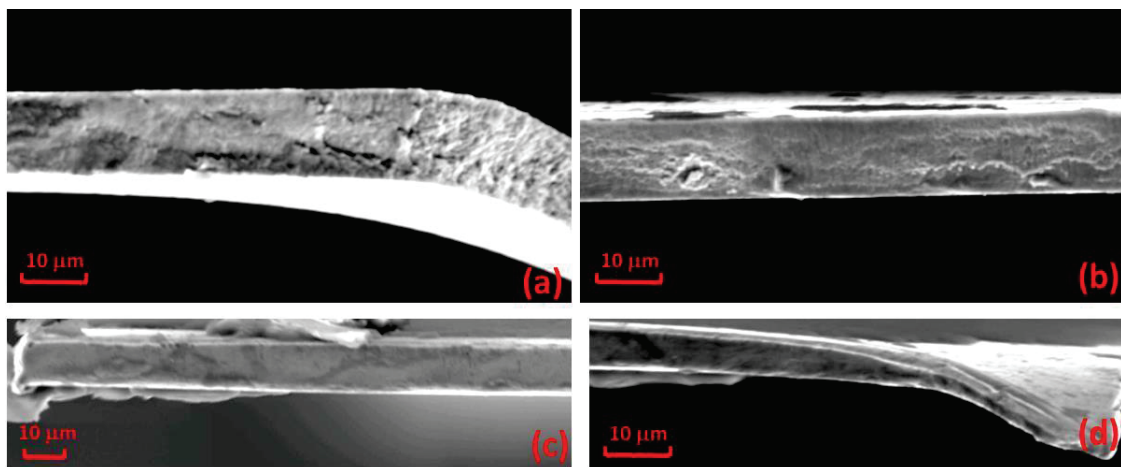


Fig. 40. Appearance of cross section of FCP test result of specimen thickness of 13 μm . (a,b,c, d) are took from rectangular A,B,C,D in Fig. 37.

3.5. Conclusions

Static tensile and tensile-tensile fatigue tests were conducted on MDFed CP Ti grade 2 thin foils with different thicknesses of; 13, 20, 30 and 50 μm . Some points could be drawn as bellow;

1. Tensile strengths of MDFed CP Ti foils are in the range of 800-1000 MPa, and higher than that of the conventional cold-rolled TP35C.
2. Fatigue limit of MDFed CP Ti foils are in the range of 200-240 MPa, and also higher than TP35C.
3. Values of tensile and fatigue strengths among the different thicknesses of MDFed CP Ti foils are scattered. There is little effect of thickness on the tensile and fatigue strengths.
4. Fatigue crack initiated from one edge of the specimen end. It indicates that few defects exist or defect free in the foils.
5. Thickness has effect on feature of the final fracture of the MDFed CP Ti thin foils. Thinner thickness reduces the colony of dimples and characterized final fracture shape into flat or slant. Flat feature appeared on 50 μ m, while the rest tends to have a slant feature.

Chapter 4 Conclusion

Titanium and titanium alloys have many good attributes such as high specific strength, low specific gravity, excellent corrosion resistance, good biocompatibility with human body. Thus they became widely used in bio medical and bio implant applications. Two main kinds of titanium for this purpose are commercially pure titanium (CP Ti) and Ti-6Al-4V. Later, there are some reports about allergic reaction on patient body with bio implant using Ti-6Al-4V. Therefore CP Ti could be more preferable than Ti-6Al-4V. However, lower mechanical strength is a kind of using and design limitation of CP Ti against heavier application.

Fortunately, this limitation was already broken up by the introduction of severe plastic deformation (SPD) techniques on CP Ti. One of these techniques is Multi-directionally Forging (MDF). For using materials as structural components like bio implant attached to human bone or tooth, they will experience continuous cyclic loading. Therefore fatigue behavior of multi-directionally forged (MDFed) CP Ti should be well understood. In this study, CP Ti grade 2 was fabricated by MDF in the shape of thin plate and thin foils. This thesis explained the fatigue behavior of MDFed CP Ti Grade 2 thin plate in the laboratory air and in simulated body fluid, namely in this case Ringer's Solution. Other explanation was about tensile properties

and fatigue behavior of MDFed CP Ti thin foil. Through this research, some points were achieved.

First, CP Ti grade 2 thin plate with the thickness of 1 mm was fabricated by MDF. Those plates of MDFed CP Ti could be used in structural component in bio implant for bone and dental application. Mainly, this bio implant should endure cyclic loading or sometimes impact loading. The MDF on CP Ti results in homogenous ultra-fine grained microstructure with the average grain size about 200 nm. This microstructure is much finer than the conventional cold-rolled commercially pure titanium TP35C. Finer microstructure not only leads to higher mechanical strength but also to higher ductility of CP Ti. That is an excellent combination of mechanical properties. The MDFed CP Ti plates are took from 3 different lots with different hardness. Higher hardness of the lots provides higher fatigue strength, and all their fatigue strengths are higher than TP35C. The improvement of fatigue strengths also could be attributed to the ultra-fine grained structure after MDF. Furthermore, the refinement of microstructure has no impact on fatigue properties against corrosive environment simulating human body, because both S-N curves in laboratory air and Ringer's solution are the same. No deterioration in corrosion resistance of CP Ti occurred even after MDF.

Fatigue fracture surfaces showed that crack typically initiated from the surface in both TP35C and MDFed CP Ti. There are exceptional cases on MDFed CP Ti which failed at the cycles longer than 10^6 cycles, namely a high cycle fatigue (HCF) region. The crack initiated from subsurface (interior) of the specimen with a feature of fish-eye. Unlike the fish-eye observed in the fatigue fracture of high strength steels, there is no inclusion at the center of fish-eye. Only titanium was detected at the center of fish-eye. It becomes one novelty in this study.

By further investigation using EBSD technique, some coarse grains with the size of a few micrometers were found in the inner part of MDFed CP Ti plate. It is a much bigger structure than the general microstructure of 200 nm. This inhomogeneity might lead to the subsurface crack initiation. In addition, the fish eye structure was also found at MDFed CP Ti at very high cycle fatigue (VHCF) region.

Second, CP Ti grade 2 thin foils with different thicknesses were fabricated by MDF. The foils have 4 different thicknesses i.e. 13, 20, 30 and 50 μm . Producing less in thickness enables it to be more wide and sensitive application of MDFed CP Ti, mainly for bio implant in dental application. The MDFed CP Ti thin foils provide tensile strengths in the range of 830-1050 MPa. Similar to the MDFed CP Ti thin plate, these values are higher than the conventional cold-rolled TP35C of 746 MPa.

More details, values of mechanical strengths are scattering among the thin foils. Thickness of 13 μ m has equal strength with 30 μ m in \sim 1050 MPa, followed by the thickness of 20 μ m in \sim 930 MPa and the less strength of \sim 830 MPa of 50 μ m. The same manners are also seen in the fatigue strengths. Fabrication by MDF had succeeded increase of fatigue strengths into the range of 200-240 MPa, higher than TP35C of 180 MPa. Scattering of fatigue strengths could be listed as follows; the highest value at 240 MPa of thickness of 30 μ m, then 230 MPa of 50 μ m, 220 MPa of 13 μ m, and 200 MPa of 20 μ m. Therefore, there is no clear effect of thickness on the tensile and fatigue strengths.

All the fatigue cracks initiated from the surface of one end of the specimen. Then crack propagated to other end of the specimen. Unlike, the MDFed CP Ti grade 2 thin plates, no sub surface crack initiation appeared in thin foils. It may indicate that only a few defects exist or even nearly defect free in the foils. Less thickness means less or no internal defect. Cross section of the fracture surface also showed that thickness of 13 μ m had only a few dimples, while 20 μ m had several dimples, and 30 and 50 μ m had many dimples. This less defect might be related to the high strengths of MDFed CP Ti. Area near the crack initiation site mostly appeared as step-like rough surface. Crack propagation area was marked by dimples or inner

slant line along width direction. Most of dimples developed till final fracture area. The final fracture appearance was characterized with the thickness of the specimens, where the thickness of 50 μ m showed a flat feature while the rests tend to had slants.

Overall, experimental results revealed that plate and foils of CP Ti grade 2 fabricated by MDF are good choice for implant application. Their mechanical strengths are nearly equal to Ti-6Al-4L/ELI, which are most widely used in biomedical or bio implant applications. Even MDFed CP Ti seems to have larger ductility that favorable for metal working of the product. Fatigue strengths of MDFed CP Ti are also higher than those of conventional cold-rolling process CP Ti, for example TP35C, but still lower than Ti-6Al-4V (rotating bending test). According to Niinomi [5], most of existing biomedical device and bio implant are made by casting, rolling, super plastic forming, and some heat treatment. Fortunately MDF is promising to apply on wide range material, even on the brittle metals. This research should be useful for the consideration of wider using of CP Ti for biomedical or bio implant need.

Although homogenous nanostructure of bulk CP Ti grade 2 had been achieved through MDF, sub-surface crack initiation with fish-eye occurred at HCF and VHCF regime of the thin plate with the thickness of 1 mm. The main reason was

weak inhomogeneity of microstructure at inner part of the thin plate. However, this fish-eye does not appear in thin foils with much less thickness. It will be a challenge to overcome this problem, to ensure more homogenous nanostructure in thin plate. This work might be related to proper work condition of making thin plate that could contribute to the rolling process design.

References

- [1] <http://www.prosperity.com/rankings?pinned=&filter=> accessed at 13 April 2018
- [2] [http://devpadhealthcare.com/Home/fracture and polytrauma](http://devpadhealthcare.com/Home/fracture%20and%20polytrauma), by 9 April 2018.
- [3] M. Saini, Y. Singh, P. Arora, K. Jain, Implant biomaterials: A comprehensive review, World Class Journal of Clinic Case 3 (2015) 52-57.
- [4] [https://www.wife.no/en/ife/departments/materials and corrosion tech/files/facts-and-figures-for-commonly-used-titanium-alloys](https://www.wife.no/en/ife/departments/materials%20and%20corrosion%20tech/files/facts-and-figures-for-commonly-used-titanium-alloys), by 2 February 2018
- [5] M. Niinomi, Mechanical properties of biomedical titanium alloys, Materials science and engineering A 243 (1998) 231-236.
- [6] M. Anuwar, R. Jayaganthan, V.K. Tewari, N. Arivazaghan, A study on the hot corrosion behavior of Ti-6Al-4V alloy, Materials letters 61 (2007) 1483-1488
- [7] M.N. Gungor, I. Ucock, L.S. Kramer, H.Dong, N.R. Martin, W.T. Tack, Materials science and engineering A 410-411 (2005) 369-374.
- [8] Y.Estrin, A. Vinogradov, Extreme grain refinement by severe plastic deformation: A wealth of challenging science, Acta materialia 61 (2013) 782-817.
- [9] Valiev RZ, Estrin Y, Horita Z, Langdon TG, Zehetbauer MJ, Zhu YT, Producing bulk ultra- fined grain materials by severe plastic deformation, JOM 58 Issue 4 (April 2006) 33-39.
- [10] X. Zhao, X. Yang, X. Liu, X. Wang, T.G. Langdon, The processing of pure titanium through multiple passes of ECAP at room temperature, Materials science and engineering A 527 (2010) 6335-6339.
- [11] H. Shahmir, P Hendrique, R. Pereira, Y Huang, TG Langdon, Mechanical properties and microstructural evolution of nanocrystalline titanium at elevated temperatures, Materials science and engineering A 669 (2016) 358-366.
- [12] H. Miura, G. Yu, X. Yang, Multi-directional forging of AZ61 Mg alloy under decreasing temperature conditions and improvement of its mechanical properties, Materials science and engineering A 528 (2011) 6981-6992.
- [13] H. Kitahara, S. Matsushita, M. Tsushida, S. Ando, N. Tsuji, Fatigue properties of ARB-processed Ti sheets with crystallographic texture, International journal of fatigue 92 part 1 (2016) 18-24.

- [14] Kaibyshev, Grain refinement in commercial alloys due to high plastic deformations and phase transformations, *Journal of materials processing technology* 117 (2001) 300-306.
- [15] Y. Nakao, H.Miura, Nano-grain evolution in austenitic stainless steel during multi-directional forging, *Materials science and engineering A* 528 (2011) 1310-1317.
- [16] A. Belyakov, K. Tsuzaki, H.Miura, T. Sakai, Effect of initial microstructures on grain refinement in a stainless steel by large strain deformation, *Acta materialia* 51 (2003) 847-861.
- [17] A. Takayama, X.Yang, H.Miura, T. Sakai, Continuous static recrystallization in untrafine-grained copper processed by multi-directional forging, *Materials science and engineering A* 478 (2008) 221-228
- [18] V. Crupi, G. Epasto, E. Guglielmino, A. Squillace, Influence of microstructure [α + α and β] on very high cycle fatigue behavior of Ti-6Al-4V alloy, *International journal of fatigue* 95 (2017) 64-75.
- [19] R.B. Osman, M.V Swain, A critical review of dental implant materials with an emphasis on titanium versus zirconia, *Materials* 8 (2015), 932-958.
- [20] C. Fleck, D. Eifler, Corrosion, fatigue and corrosion fatigue behavior of metal implant materials, especially titanium alloys, *International journal of fatigue* 32(2010) 929-935.
- [21] N. Hoshi, M. Saita, T. Kumasaka, M. Banka, H. Miura and K. Kimoto: *The Journal of the Japanese Society for Dental Materials and Devices* 32 (2013) 403. (in Japanese).
- [22] Tonichi Shimbun News, <http://datazenkokunews.com/201405/26/2014-05-26-tonichi.pdf>, (accessed 2018-04-26). (in Japanese)
- [23] G.S. Dyakonov, S.V. Zhherebtsov, S.P. Malysheva, G.A. Salishchev, A.A.Salem and S.L.Semiatin, *Materials science and engineering A* 607(2014) 145-154
- [24] Ilhamdi, Y.Uematsu, T.Kakiuchi, T.Shimizu, Y.Nakamura and M.Nakajima, *Proceeding of JSME annual meeting*, (The Japanese Society of Mechanical Engineers, 2017) No. 17-1 (CD-ROM). (in Japanese).
- [25] T. Abe, Y. Furuya, S. Matsuoka, Gigacycle fatigue properties of 1800 Mpa class spring steels, *Fatigue fracture engineering material structure* 27 (2004) 159-167
- [26] A. Roiko, Y. Muarakami, A design approach for components in ultralong fatigue life with step loading, *International journal of fatigue* 41(2012) 140-149.

- [27] Y. Uematsu, K. Tokaji, H. Takekawa, Effect of thick DLC coating on fatigue behavior of magnesium alloy in laboratory air and demineralized water, *Fatigue and fracture of engineering materials & structures*, 33 (2010) 607-616.
- [28] Y. Uematsu, T.Kakiuchi, K.Hattori, EBSD-assisted fractography of sub-surface crack initiation mechanism in the ultrasonic-shot-peened beta-type titanium alloy, *fatigue and fracture of engineering materials & structures*, April 2018, DOI:10.1111/ffe.1281
- [29] H.Oguna, T.Nakamura, S.Yokoyama, T.Noguchi: *Japanese Society Materials Sciences*, Japan 52 (2003) 1298-1304. (in Japanese)
- [30] X. Liu, C. Sun, Y. Hong, Effect of stress ratio on high-cycle and very-high-cycle fatigue behavior of Ti-6Al-4V alloy, *Materials science and engineering A* 622(2015) 228-235.
- [31] S. Heinz, D. Eifler, Crack initiation mechanisms of Ti6Al4V in the very high cycle fatigue regime, *International journal of fatigue* 93 (2016) 301-308.
- [32] M.N. Gungor, I. Ucock, L.S. Kramer, H. Dong, N.R. Martin, W.T. Tack, *Materials science engineering A* 410-411 (2005) 369.
- [33] X. Song, M. Niinomi, H.Tsutsumi, M.Nakai, L.Wang, Effect of TiB on the mechanical properties of Ti-29Nb-13Ta-4.6Zr alloy for use in biomedical application, *Materials science engineering A* 528 (2011) 5600
- [34] R.R. Boyer, An overview on the use of titanium in the aerospace industry, *Materials science engineering A* 213 (1996) 104
- [35] I.V. Gorynin, Titanium alloys for marine application, *Materials science engineering A* 263 (1999) 113
- [36] X. Song, L. Wang, M. Niinomi, M.Nakai, Y. Liu, Fatigue characteristics of a biomedical b-type titanium alloy with titanium boride, *Materials science engineering A* 640 (2015) 154-164
- [37] R. Naseri, M.Kadkhodayan, M.Shariati, Static mechanical properties and ductility of biomedical ultrafine-grained commercially pure titanium produced by ECAP process, *Transaction of nonferrous metals society of China* 27 (2017) 1964-1975
- [38] V-D. Cojocaru, D. Raducanu, D.M. Gordin, I Cinca, Texture evolution during ARB (Accumulative Roll Bonding) processing of Ti-10Zr-5Nb-5Ta alloy, *Journal of alloy and compound* 546 (2013) 260-269
- [39] K. Vaclavova, J. Strasky, V. Polyakova, J. Straska, J.Nejezchlebova, H. Seiner, I. Semenova, M. Janecek, Microhardness and microstructure evolution of ultra-fine

- grained Ti-15Mo and TIMETAL LCB alloys prepared by high pressure torsion, Materials science engineering A 682 (2017) 220-228
- [40] A. Danno, C.C. Wong, S. Tong, A. Jarfors, K. Nishino, T. Furuta, Effect of cold severe deformation by multi directional forging on elastic modulus of multi functiona; Ti+25 mol% (Ta,Nb,V) + (Zr,Hr,O) alloy, Materials & design 31 (2010) S61-S65.
- [41] Ilhamdi, T. Kakiuchi, H. Miura, Y. Uematsu, High cycle fatigue properties of multi-directionally forged commercial purity grade 2 Ti plate, Material science forum 916 (2018) 166-169.
- [42] S. Fintova, M.Arzaghi,I.Kubena,Ch.Sarrazin-Baoudux, Fatigue crack propagation in UFG Ti grade 4 processed by severe plastic deformation, International journal of fatigue, 89 (2017) 187-194.
- [43] M.A.L.Hernandez-Rodriguez, G.R.Contreras-Hernadez, A.Juarez-Hernandez, B.Beltran-Ramirez, E.Garcia-Sanchez, Failure analysis in dental implant, Engineering failure analysis, 57 (201) 236-242.
- [44] G. Lütjering and J.C. Williams, Titanium, Springer, Berlin Heidelberg (2007) 175-197

List of publication

Journal

- [1] High Cycle Fatigue Properties of Multi-Directionally Forged Commercial Purity Grade 2 Ti Plate", Ilhamdi, T. Kakiuchi, H. Miura, Y. Uematsu, Materials Science Forum, Vol. 916, pp. 166-169, 2018
- [2] Fatigue behavior of multi-directionally forged commercial purity grade 2 Ti plate in laboratory air and Ringer's solution, Ilhamdi, T. Kakiuchi, H. Miura, T. Fukihara and Y. Uematsu, Materials Transactions Vol. 59 No. 8, pp. 1296 to 1303, 2018.

International conference

- [1] High Cycle Fatigue Properties of Multi-Directionally Forged Commercial Purity Grade 2 Ti Plate", Ilhamdi, T. Kakiuchi, H. Miura, Y. Uematsu, 2nd International Conference on materials Technology and Applications (ICMTA) at Tokyo University of Science, 26-29 October 2017
- [2] Fatigue properties of Multi-directionally Forged CP Titanium Thin Foil, Ilhamdi and Yoshihiko Uematsu, 3rd International Conference on Mechanical Engineering (ICOME) 2017, Surabaya Indonesia, 5-6 October 2017

National conference

- [1] Fatigue behavior of multi-directionally forged commercially pure Ti thin foil with different thickness, Ilhamdi, Y. Uematsu, H. Miura, T. Kakiuchi, T. Shimizu, Y. Nakamura, and M. Nakajima, Mechanical Engineering Congress, 2017 Japan (MECJ-17) at Saitama University, 3-5 September 2017